The role of TRPC6 in cardiac positive inotropy through sympathetic nervous system

Oda, Sayaka

The Graduate University for Advanced Studies, SOKENDAI

School of Life Science

Department of Physiological Sciences

Table of contents

Abstract

Regulation of cardiac functions, primarily left ventricular (LV) contractility (inotropy) and heart rate (chronotropy), through autonomic nervous system is indispensable for the maintenance of blood circulatory homeostasis. β adrenergic receptors (ARs) are expressed in the heart and activated by norepinephrine (NE) released from sympathetic nerve endings, which leads to induction of positive inotropic and chronotropic effects. Although β_1AR is believed to predominantly mediate NE-induced increase in cardiac functions, it is not well understood how cardiac functions are sufficiently fine-tuned by βARs, much lower-affinity binding receptors to NE than αARs. Previous reports have shown that transient receptor potential canonical (TRPC) 6 plays important roles in α_1AR-stimulated vasoconstriction and pathogenesis of heart failure in rodents. Although pathological roles of TRPC6 have been extensively studied, its physiological role is still obscure. In this research, I investigated whether TRPC6 participates in physiological cardiac responses induced by activation of autonomic nervous system.

First, cardiac and vascular responses induced by stimulation of adrenergic receptors (βAR and αAR) or muscarinic receptor (MR) were compared among wild type (WT), TRPC3- and TRPC6-deficient mice using surgical LV catheterization. I found that isoproterenol (ISO; βAR specific agonist)-induced positive inotropic effect was reduced in TRPC6-deficient mice, whereas βAR-stimulated positive chronotropic effect, αAR-stimulated transient increase in blood pressure and MR-stimulated negative inotropic and chronotropic effects were not different significantly among three groups. Proximity ligation assay (PLA) revealed that TRPC6 was in close proximity to β_1AR in ventricle cardiomyocytes, but not sinoatrial node cells. Additionally, ISO-induced increase in shortening of sarcomere length and Ca^{2+} transient were significantly reduced in isolated TRPC6-deficient adult mouse cardiomyocytes. Knockdown of TRPC6 suppressed ISO-mediated increase in intracellular cyclic adenosine

monophosphate (cAMP) production in neonatal rat cardiomyocytes (NRCMs). These results suggest that TRPC6 acts as a positive regulator of βAR-Gs signaling in cardiomyocytes. I next investigated the molecular mechanism underlying enhancement of βAR-Gs signaling by TRPC6 channel. I found that: 1) intracellular zinc ion (Zn^{2+}) pool in TRPC6-deficient cardiomyocytes was smaller than that in WT cardiomyocytes. 2) NE-induced αAR stimulation caused TRPC6-mediated Zn^{2+} influx in HEK293 cells. 3) αAR inhibition and intracellular Zn^{2+} chelation suppressed NE-induced cAMP production in NRCMs. 4) TRPC6 activation mediated by αAR stimulation enhanced ISO-induced cAMP production and this enhancement was canceled by TRPC6 knockdown in NRCMs. These results suggest that αAR-mediated Zn^{2+} influx via TRPC6 enhances βAR-Gs signaling. Finally, I examined whether TRPC6 contributes to baroreflex-induced cardiac inotropy in mice. I found that a reflex inotropy induced by hydralazine, a pharmacological vasodilator, was significantly reduced in TRPC6-deficient mice, while a coincident reflex chronotropy was not affected. I have previously reported that hyperglycemia increases TRPC6 expression in the heart. Consistently, positive inotropic effect was promoted in streptozotocin-treated hyperglycemic mice. The interaction between TRPC6 and β_1AR determined by PLA was also enhanced in the base of hyperglycemic mouse hearts. In the first section, I revealed that TRPC6 positively regulates cardiac inotropy by enhancing βAR-Gs signaling through αAR-Zn^{2+} axis.

In the second section, I investigated whether TRPC6 regulates ISO-induced βAR internalization. Co-expression of TRPC6 with β_1AR suppressed ISO-induced β_1AR internalization and β-arrestin 2 (βArr2) translocation to the plasma membrane in HEK293 cells. Basal interaction between β_1AR and βArr2 was significantly reduced in TRPC6-deficient mouse cardiomyocytes, indicating that TRPC6 is involved in ligand-stimulated βAR internalization process.

In the third section, I investigated whether TRPC6 contributes to the progression of cardiac remodeling caused by chronic βAR activation. Subcutaneous administration with ISO continuously

for 4 weeks induced LV remodeling and dysfunction in WT mice, while ISO-induced heart failure was suppressed in TRPC6-deficient mice. In contrast, ISO-induced increase in heart weight was enhanced in TRPC6-deficient mice. In fact, chronic βAR activation enhanced TRPC6 mRNA expression in mouse hearts. Thus, TRPC6 contributes to βAR-induced heart failure and negatively regulates cardiac hypertrophy in mice.

Collectively, I revealed that TRPC6 links between αAR and βAR through Zn^{2+} mobilization, leading to enhancement of cardiac positive inotropy in response to sympathetic nerve activation. Since TRPC6 is expressed universally and various biological responses are regulated by sympathetic nervous system, Zn^{2+}-dependent enhancement of βAR signaling via TRPC6 might be involved in other physiological responses.

Abbreviation

ACh	Acetylcholine
AR	Adrenergic receptor
cAMP	Cyclic adenosine monophosphate
BRET	Bioluminescence resonance energy transfer
DTDP	2,2′-dithiodipyridine
FRET	Förster resonance energy transfer
FS	Fractional shortening
HCN4	Potassium/sodium hyperpolarization-activated cyclic nucleotide-gated channel 4
ISO	Isoproterenol
LV	Left ventricle
NE	Norepinephrine
PLA	Proximity ligation assay
RV	Right ventricle
SAN	Sinoatrial node
STZ	Streptozotocin
TPEN	N,N,N',N'-Tetrakis(2-pyridylmethyl)ethylenediamine
TRPC	Canonical transient receptor potential
WGA	Wheat germ agglutinin

Introduction

The heart pumps blood throughout circulatory system and delivers substances necessary for survival such as oxygen, nutrients and humoral factors. Once internal or external environments change, the heart alters its function to keep blood supply and meet each tissue and organ's demand consistently, which maintains systemic oxygen homeostasis. Therefore, the precise regulation of cardiac functions (such as pumping power and heart rate) is essential for survival. The autonomic nervous system is mainly involved in this regulation. The autonomic nervous system is divided into two nervous systems: the sympathetic nervous system (promoting "fight-or-flight" responses) and the parasympathetic nervous system (promoting "rest and digest" responses). In the sympathetic nervous system, norepinephrine (NE) is released from nerve endings and binds to α and β adrenergic receptors (AR). There are 7 αAR (α_{1A}, α_{1B}, α_{1D}, $\alpha_{2A\text{-}D}$) and 3 βAR (β_1, β_2, β_3) subtypes, and β_1AR and β_2AR are predominantly expressed in the heart [1]. Activation of βAR elicits a positive inotropic effect (increase of cardiac contractility) and a positive chronotropic effect (increase in heart rate). αAR is mainly expressed in vascular smooth muscle cells and their activation promotes vasoconstriction. Although αAR is expressed in the heart, their expression level is quite low (αAR: βAR=1:9) [2]. Previous studies have shown that αAR activation induces a positive or negative inotropic effect dependently on αAR subtypes or experimental conditions, which makes it difficult to determine the roles of αAR in cardiac function [3,4]. In human heart, treatment with α_1AR antagonist does not affect basal cardiac contractility, indicating that contribution of αAR to basal cardiac function is small [5]. On the other hand, acetylcholine (ACh) is released from parasympathetic nerve endings and binds to muscarinic receptor (M2 subtype). Activation of muscarinic receptors produces negative inotropic and chronotropic effects. Cardiac contractility and heart rate are flexibly regulated by keeping the balance between sympathetic nervous system and parasympathetic nervous system. Although a lot of researchers have investigated

how cardiac functions are regulated at molecular levels for a long time, the mechanism is quite complicated and not fully understood. For instance, it is not clear how cardiac functions are sufficiently fine-tuned by βARs, much lower-affinity binding receptors to NE than αARs.

One of the most important molecular mechanisms for regulation of cardiac functions is the control of intracellular ion concentration, especially calcium ion (Ca^{2+}). Cardiac contraction is mediated by excitation-contraction coupling (E-C coupling) driven by Ca^{2+} influx through L-type Ca^{2+} channels. A periodic electrical excitation of surface membrane (action potential) triggers Ca^{2+} influx via voltage-gated L-type Ca^{2+} channels, which leads to Ca^{2+} release from sarcoplasmic reticulum. Once intracellular free Ca^{2+} concentration is increased, Ca^{2+} binds to troponin C and allows interaction between actin and myosin filament, resulting in contraction of cardiomyocytes. Rise in intracellular Ca^{2+} concentration is restored by pumps and transporters such as sarco/endoplasmic reticulum Ca^{2+}-ATPase (SERCA) and sodium-calcium exchanger (NCX). Repetition of these rapid increase and decrease in global Ca^{2+} concentration determines rhythmical cardiac contraction and relaxation. On the other hand, there is an alternative (local) Ca^{2+}-mediated signaling pathway which works for Ca^{2+}-dependent gene expression: excitation-transcription coupling (E-T coupling). In this pathway, Ca^{2+} influx through receptor-operated Ca^{2+} channel (ROCC) or mechano-activated Ca^{2+} channel play an important role. This local Ca^{2+} influx is evoked by chemical (e.g. extracellular neurotransmitters, humoral factors) and physical stimulations (e.g. mechanical stress, shearing stress), and activates Ca^{2+}-dependent transcription factors (e.g. nuclear factor of activated T cells (NFAT), myocyte enhancer factor (MEF)), which leads to gene expression. E-T coupling is involved in chronic cardiac remodeling (morphological change for adaptation) and accompanying cardiac dysfunctions. Transient receptor potential (TRP) proteins, especially canonical TRP (TRPC) subfamily members, are considered to function as ROCC [6].

TRP protein was initially identified in visual phototransduction mutant strain of *Drosophila*

melanogaster in 1989 [7]. Based on sequence homology and functional similarity, 28 mammalian TRP homologs are classified into 6 subfamilies; TRPC (canonical), TRPV (vanilloid), TRPM (melastatin), TRPP (polycystin), TRPML (mucolipin) and TRPA (ankyrin) [8]. TRP protein has two unique functions. One is a function as "sensor". TRP channel is activated by various extracellular stimuli (e.g. chemical substances, physical stress, temperature, pH) directly or indirectly and transmits the signal into the cell accurately through cation influx. The other is a function as "protein scaffold" [9]. TRP proteins interact with multiple proteins and form a signaling platform. These features enable a spatiotemporal regulation and amplification of signal transduction.

TRPC subfamily comprises 7 isoforms (TRPC1-7) which is highly homologous to the original *Drosophila* TRP channel. TRPC channels are activated downstream of Gq-coupling receptor signaling [10]. All TRPC isoforms except TRPC2 (pseudogene) are expressed in human heart. Among these isoforms, TRPC3 and 6 share common features. TRPC3 and TRPC6 show high homology covering ~75% of amino acid sequence [11]. TRPC3 and 6 form not only homo-tetramer channel but also hetero-tetramer channel by interacting with each other [12] and activated by diacylglycerol directly [13]. Previous studies have reported that both "sensor" function and "scaffold" function of these channels are involved in pathological cardiac remodeling [14]. TRPC3 and 6 mediate angiotensin II-induced hypertrophy in neonatal rat cardiomyocytes (NRCMs) [15] and cardiac dysfunction induced by pressure overload in mice [16]. Cardiomyocyte-specific overexpression of TRPC3 or TRPC6 increases sensitivity to pressure overload, leading to deterioration of cardiac functions [17,18]. Furthermore, mRNA expression levels of TRPC3/6 are increased in human failing hearts [18,19]. TRPC3 and 6 are seemingly considered to play similar roles in the heart. However, we have reported that TRPC3 interacts with NADPH oxidase 2 (Nox2) and promotes production of reactive oxygen species (ROS) in pressure-overloaded hearts and atrophied NRCMs induced by ATP [20,21], whereas TRPC6 suppresses formation of TRPC3-Nox2 complex and ROS production in hyperglycemic hearts [22], indicating that TRPC3 and 6 may have

different functions in the heart. Although both TRPC3 and TRPC6 are certainly essential for the pathogenesis of heart failure, physiological roles of TRPC3/6 are still obscure due to their functional redundancy. Indeed, mice which lack all TRPC homologs were born and live normally [23]. Therefore, I investigated the physiological role of TRPC3/6 channels, by focusing on adaptive changes in cardiac functions through autonomic nervous system.

Materials and Methods

Reagents and antibodies

(−)-Isoproterenol hydrochloride (ISO, I6504), acetylcholine chloride (ACh, A6625), (±)-norepinephrine (+)-bitartrate salt (NE, A0937), 2,2′-dithiodipyridine (DTDP, D5767), prazosin hydrochloride (P7791), (±)-propranolol hydrochloride (P0884), methoxamine hydrochloride (M6524) and streptozotocin (STZ, S0130) were purchased from Sigma Aldrich. Fluo 4-AM (F311), Fura 2-AM (F016) and N,N,N',N'-Tetrakis(2-pyridylmethyl)ethylenediamine (TPEN, 343-05401) were from Dojindo. FluoZin™-3 AM (F24195) was from Thermo Fisher. 1-Hydrazinophthalazine hydrochloride (hydralazine hydrochloride, H0409) and isoproterenol hydrochloride (for chronic injection, I0260) were from Tokyo Chemical Industry. A list of the antibodies used are given in Table 1.

Animals

All protocols using mice and rats were reviewed and approved by the ethics committees at the National Institutes of Natural Sciences and carried out in accordance with their guidelines (20A049, 20A050). 129/Sv mice with homozygous deletion of gene encoding TRPC6 and TRPC3 were provided by the Comparative Medicine Branch, National Institute of Environmental Health Sciences, Research Triangle Park, Noeth Carolina 27709. Genotyping was performed as previously described [24,25]. All mice were maintained in specific-pathogen-free area under a 12-h light/dark cycle. Sprague-Dawley rats were purchased from Japan SLC, Inc.

Animal model

For induction of hyperglycemia, male mice (8-9 weeks old) were injected intraperitoneally with STZ at a dose of 50 mg/kg body weight (dissolved in 0.1 M citrate buffer, pH 4.5) for 5 consecutive

days. Control mice were injected with an equal volume of 0.1 M citrate buffer. In ISO chronic injection experiment, ISO was dissolved in phosphate-buffered saline (PBS) which contained 0.1% ascorbic acid and subcutaneously infused in male mice (9-11 weeks old) at 30 mg/kg with an osmotic mini pump (Alzet, 2004).

Measurement of cardiac function

Hemodynamic parameters were measured using a micronanometer catheter (Millar 1.4F, SPR 671, Millar Instruments). Mice were anesthetized with isoflurane (Pfizer) at a concentration of 2.0-2.3% for induction. After insertion of catheter to left ventricular (LV) chamber, isoflurane concentration was lowered to 1.5-1.7% for maintenance. To maintain hemodynamic parameters constant before agonist infusion, measurements were started at least 10 min after change to maintenance concentration. For analyzing responses to receptor stimulation in the autonomic nervous system, ISO (10 pg/g/min, 0.05 mL/h), ACh (0.5 mg/kg, 1.8 mL/h) were injected to mice and LV parameters were measured. To measure hemodynamic parameters in blood vessel, a catheter was inserted to the aorta and mice were injected with NE (0.05 mg/kg, 1.8 mL/h). For analyzing reflex responses, hydralazine (0.5 mg/kg, 1.2 mL/h) was injected to mice. Compound injection to mice was from jugular vein using cannula made of polyethylene tube (internal diameter 0.28 mm) and syringe infusion pump (KDS100, KdScientific). Results were calculated as follows: average values of each parameter before injection were subtracted from values of each time point after injection. These subtracted values were shown as Δ. Echocardiography was performed using Nemio XG echocardiography (Toshiba) with a 14-MHz transducer under anesthesia with isoflurane (2.0-2.5% for induction).

Isolation of adult mouse ventricular cardiomyocytes

Isolation of adult mouse ventricular cardiomyocytes was performed as described previously [26].

Briefly, male mouse was heparinized (>100 units per mice, i.p.) and anesthetized (pentobarbital sodium, >300 mg/kg). Heart was quickly excised and the aorta was clamped with a small vascular clamp. Clamped heart was antegradely perfused with isolation buffer (containing (in mM) 130 NaCl, 5.4 KCl, 0.5 $MgCl_2$, 0.33 NaH_2PO_4, 25 HEPES, 22 glucose and 50 μU/mL bovine insulin (Sigma) (pH 7.4, adjusted with NaOH)) supplemented 0.4 mM EGTA and followed by isolation buffer containing in addition 1 mg/mL collagenase type 2 (Worthington), 0.06 mg/mL trypsin (Sigma), 0.06 mg/mL protease (Sigma) and 0.3 mM $CaCl_2$. Thereafter, the LV chamber was removed and cut into small pieces in enzyme solution containing 0.2% bovine serum albumin (BSA) and 0.7 mM $CaCl_2$. The tissue-cell suspension was filtered through a cell strainer (100 μm, Falcon) and centrifuged for 3 min at 300 rpm. After removing supernatant, the cell pellet was resuspended in isolation buffer supplemented with 0.2% BSA and 1.2 mM $CaCl_2$ and incubated for 10 min at 37°C. After final centrifugation (300 rpm, 3 min), the cells were resuspended in tyrode solution A (containing (in mM) 140 NaCl, 5.4 KCl, 1.8 $CaCl_2$, 0.5 $MgCl_2$, 0.33 NaH_2PO_4, 5.0 HEPES and 5.5 glucose (pH 7.4)) supplemented with 0.2% BSA. Cells were seeded to matrigel (Corning)-coated 35mm glass base dishes (glass 12Φ, IWAKI) or glass slides and incubated at 37°C for 1 h. Cells were used within 1-6 h after isolation.

Isolation of neonatal rat cardiomyocytes, cell culture and transfection

Neonatal rat cardiomyocytes (NRCMs) were isolated from Sprague-Dawley rat pups on postnatal day 1-2. First, pups were sacrificed and dissected ventricles were minced. The minced tissue was pre-digested in 0.05% trypsin-EDTA (Gibco) overnight at 4°C and then digested in 1 mg/mL collagenase type2 (Worthington) in PBS for 30 min at 37°C while shaking the flask (125 rpm). The dissociated cells were filtered through a cell strainer (70 μm, Falcon) and centrifuged for 2 min at 180 xg. After removing supernatant, cell pellets were resuspended in Dulbecco's modified Eagle's medium

(DMEM) supplemented with 10% FBS and 1% penicillin and streptomycin plated in a 10-cm culture dish. Cells were incubated at 37°C in a humidified atmosphere (5% CO_2, 95% air) for 90 min. Floating NRCMs were collected and plated to matrigel-coated culture dishes. After 24 h, the culture medium was changed to serum-free DMEM and incubated for more than 2 days before experiments. For gene knockdown, the cells were transfected with siRNAs (20 nM) for 72 h using Lipofectamine RNAiMAX (Invitrogen™). Stealth siRNAs for rat TRPC6 (#1, RSS331768; #2, RSS331769) and Stealth RNAi™ siRNA negative control (med GC) for siControl were from Invitrogen™. Plasmid DNA was transfected using Lipofectamine 3000 (Invitrogen™) 1 day after siRNA transfection and cells were incubated for 48 h.

HEK293 cell culture and transfection

HEK293 cells were cultured in DMEM supplemented with 10% FBS and 1% penicillin and streptomycin. Cells were seeded at a density of 5×10^5 cells/dish in 35 mm dish. Plasmid DNAs were transfected with X-tremeGENE9 (Roche) the day after seeding and cells were incubated for 48 h. For imaging experiments, cells were replated on poly-L-lysine (Sigma)-coated glass coverslips or 35mm glass base dishes (glass 12Φ) 1 day before experiment.

Measurement of cardiomyocyte sarcomere length and calcium transient

The detailed method for performing sarcomere length (SL) measurement is described previously [27-29]. Briefly, isolated cells were stored in solution A containing (in mM) 128 NaCl, 2.6 KCl, 1.18 $MgSO_4$, 1.18 KH_2PO_4, 1.8 $CaCl_2$, 10 HEPES, 20 taurine and 11 glucose (pH 7.4). The myocytes were monitored through an inverted microscope (IX-70; Olympus) using a 40× long working distance objective lens (LUCPLN40×; Olympus). The cells were placed on a poly- HEMA (2-hydroxyethyl methacrylate; P3932, Sigma)-coated coverslip to prevent firm cell attachment to the bottom of the

chamber. One of the cell ends was held by a short carbon fiber mounted in a glass capillary manipulated using a three-axis hydraulic manipulator (EDMS14-135a; Narishige), to prevent cells from being swept out of the field of view by the perfusate during the measurement. After holding the cell with the carbon fiber, the cell was perfused in tyrode solution B containing (in mM) 140 NaCl, 5.4 KCl, 1.8 $CaCl_2$, 1.0 $MgCl_2$, 5.0 HEPES and 11 glucose (pH 7.4) at 37°C using an MPRE8 in-line heater (Cell Microcontrols) and electrically stimulated at 4 Hz using a MyoPacer cell stimulator (IonOptix Corporation). The myocyte SL changes were recorded at 240 Hz, using IonOptix hardware and software (IonOptix Corporation). After recording a stable SL traces in tyrode solution B without any drugs (control), the perfusion solution was changed into tyrode solution B containing 10 nM ISO using a valve-controlled gravity perfusion system (VC3-4PG; ALA Scientific Instruments). The SL recording was conducted until obtaining the steady myocyte contraction in existence of ISO. Data was provided by Dr. Y. Yamaguchi and Prof. G. Iribe (Asahikawa Medical University).

For Ca^{2+} transient measurements, cardiomyocytes were loaded with Fluo 4-AM (2 μM) for 30 min at 37°C after washing with tyrode solution A. Measurement of Ca^{2+} transient was performed at 1 Hz pacing frequency with a pulse of 10 msec duration using a pair of platinum wires placed on opposite sides of the chamber, which is connected to an electrical stimulator (SEN-3301, NIHON KOHDEN). Cells were stimulated with ISO (10 nM). Images were acquired at a rate of 5 Hz and analyzed using a video image analysis system (Metafluor, Molecular Devices).

Zinc and calcium imaging experiments

For analyzing changes in the intracellular free Zn^{2+} concentration in adult mice cardiomyocytes, isolated cells from WT/TRPC6$^{(-/-)}$/TRPC3$^{(-/-)}$ mice were seeded to matrigel-coated glass base dishes. Cells were washed with tyrode solution A and loaded with the fluorescent Zn^{2+} indicator FluoZin-3 (2 μM) for 30 min at 37°C. Cells were treated with DTDP (100 μM) 2 min after starting the experiment.

Images were acquired every 10 sec and analyzed using Metafluor.

For measurement of Zn^{2+} influx, HEK293 cell were transfected with α_{1A}AR, mCherry vector or TRPC6/3-mCherry. Cells were washed with HEPES-buffered saline solution (HBSS) containing (in mM) 140 NaCl, 5.6 KCl, 10 glucose, 10 HEPES 1 $MgCl_2$ and 1.8 $CaCl_2$ (at pH 7.4) and loaded with FluoZin-3 (2 μM) for 30 min at room temperature. After loading, the dye solution was then replaced with HBSS. $ZnCl_2$ (50 μM) was applied to bath 2 min after starting measurement. As α_{1A}AR agonist, NE (10 μM) was added 3 min after $ZnCl_2$ application. Fluorescence images were acquired every 10 sec using a confocal microscope (TCS SP8 MP, Leica). For analysis, mCherry-positive cells were selected.

For measurement of Ca^{2+} influx, HEK293 cells were transfected with α_{1A}AR or hemagglutinin -tagged βAR (HA-βAR) along with mCherry vector or TRPC6/3-mCherry. Cells were washed with HBSS and loaded with Fura-2 (1 μM) for 30 min at room temperature. Thereafter, cells were washed with HBSS and stimulated with ISO (10 μM) 2 min after the starting the experiment. Fluorescence images were acquired every 10 sec using Metafluor. For analysis, Fura-2 signals (F340 nm/F380 nm) were measured in mCherry-positive cells.

cAMP measurements

For FRET imaging, NRCMs were seeded to matrigel-coated glass base dishes the day before siRNA transfection. Cells were transfected siControl, siTRPC6-1 or siTRPC6-2 and also transfected Epac-based FRET sensor (Epac-S^{H187}; high affinity version) 1 day after siRNA transfection. The biosensor was gifted by Prof. K. Jalink [30]. Cells were washed by HBSS and stimulated with ISO (1 μM) 2 min after starting the experiment. Images were captured every 10 sec using TCS SP8 MP. FRET was expressed as ratio of CFP to YFP signals.

For ELISA experiment, NRCMs seeded to matrigel-coated 12 or 24-well plate. After incubating in

serum-free DMEM for 24-48 h or treatment of siRNA, cells were treated with prazosin (10 μM), propranolol (10 μM) and methoxamine (1 μM) for 24 h with extracellular $ZnCl_2$ (50 μM). Thereafter, cells were treated with 3-isobutyl-1-methylxanthine (IBMX; 500 μM, Sigma) for 1 h in the presence of each compound, following NE (1 μM) or ISO (1 μM) stimulation for 30 min. In TPEN group, TPEN (25 μM) was added with IBMX. Control group was treated with DMSO. After stimulation, culture medium was removed on ice and cells were lysed by adding 0.1 M HCl (200 μL for 12-well plate; 100 μL for 24-well plate), following incubation for 20 min at room temperature. Cell suspension was collected and centrifuged for 10 min at 1,000 xg. Intracellular cAMP levels were measured using cAMP EIA Kit (Cayman Chemical) according to manufacturer's instruction.

Immunostaining and proximity ligation assay

Mouse heart tissues were embedded in optimal cutting temperature (O.C.T.) compound (Sakura Finetek) and snap-frozen in bath of cooled 2-methylbutane by dry ice. 12-μm-thick sections were cut on a cryostat. Isolated adult mice cardiomyocytes were plated on matrigel-coated glasses. Immunostaining was performed as follows: glass-mounted cryosection were fixed in 4% paraformaldehyde (PFA, dissolved in 1% PBS) for 7 min at room temperature. After rinsing with PBS, sections were blocked in PBS with 0.1% BSA, 0.3% Triton X-100 at room temperature for 1 h and then incubated with primary antibodies overnight at 4°C, following labeling by Alexa Fluor™ dye-conjugated secondary antibodies and Alexa Fluor™ 488-conjugated wheat germ agglutinin (WGA; Thermo Fisher). Samples were mounted with ProLong™ Diamond Antifade Mountant with DAPI (Thermo Fisher). To determine TRPC6-β_1AR interaction and β_1AR-β-arrestin 2 (βArr2) interaction, proximity ligation assay (PLA) was conducted using Duolink PLA Fluorescence (Sigma) according to the manufacturer's instruction. After fixing and blocking, heart sections and cardiomyocytes were incubated with rabbit anti-β_1AR and mouse anti-TRPC6 or anti-βArr2 for 2 overnights at 4°C,

followed by 1 h PLA probes incubation. The ligation (30 min) and amplification (150 min) steps were performed at 37°C chamber and samples were counterstained with Alexa Fluor™ 488-conjugated WGA (for heart section) or Alexa Fluor™ 488-conjugated phalloidin (Thermo Fisher, for adult mice cardiomyocyte), and nuclear stained with DAPI. Images were captured using a confocal microscope (A1Rsi, Nikon) or BZ-X700 fluorescence microscope (Keyence). The number of PLA signal-positive puncta were quantified and analyzed using ImageJ (National Institutes of Health) software.

Morphological analysis of mouse hearts

For preparation of paraffin sections, dissected hearts were rinsed in cold PBS and fixed in 10% neutral-buffer formalin at least overnight. Sections were cut at 3 μm thickness and stained with hematoxylin and eosin (H&E). Images were captured using BZ-X700 fluorescence microscope and cross-sectional area (CSA) was analyzed using ImageJ software.

Measurement of biochemical parameters

In STZ model, non-fasted blood glucose levels were determined by Glucose Pilot (Technicon) 4 weeks after STZ injection. For analyzing plasma sample after 4-week ISO injection, blood samples were collected from inferior vena cava and centrifuged at 3,000 xg for 10 min to prepare plasma samples. Plasma biochemical parameters were measured using DRI-CHEM NX500 (Fuji Film) according to manufacturer's instruction.

Radioligand Binding Assay

Mouse heart tissues were homogenized in homogenate buffer (25 mM Tris-HCl (at pH 7.4) and 2 mM EDTA) using a physcotron homogenizer. The homogenate was centrifuged at 800 xg for 10 min at 4°C. The supernatant was ultracentrifuged at 125,000 xg for 30 min at 4°C. The pellet was

resuspended in assay buffer (75 mM Tris-HCl (at pH7.4), 2 mM EDTA and 12.5 mM $MgCl_2$) using a Dounce homogenizer. For receptor binding assay, tubes with 50 μg protein in a total volume of 200 μL of assay buffer with or without 20 μM propranolol were used. Tubes were incubated with the radiolabeled antagonist [^{125}I]CYP (final concentration 12.5-400 pM) for 90 min at 30°C. The reactions were stopped by the addition of an ice-cold assay buffer and filtered through Whatman GF/C glass microfiber filters presoaked in 0.1% polyethylenimine. The filters were washed three times with an ice-cold assay buffer and air-dried. The radioactivity was measured using liquid scintillation counter. Radioligand binding assay was performed by Dr. A. Nishimura (National Institute for Physiological Sciences).

RNA isolation and RT-PCR

Total RNA was isolated from frozen mouse hearts and NRCMs using RNeasy Fibrous Tissue Mini Kit (Qiagen) according to the manufacturer's instruction. Complementary DNA was synthesized with ReverTra Ace® qPCR RT Master Mix (TOYOBO). Real-time polymerase chain reaction (RT-PCR) was performed using Lightcycler® 96 (Roche) with KAPA SYBR® FAST qPCR kit (KAPA BIOSYSTEMS) according to the manufacturer's instructions. The primer sequences used for RT-PCR are listed in Table 2.

Microarray analysis

Microarray analysis was performed as described previously [31]. Briefly, RNA samples were converted into biotinylated cRNA using Two-Cycle Target Labeling and Control Reagents (Thermo Fisher). Labeled RNA was processed for microarray hybridization to GeneChip Mouse Genome 430 2.0 array (Thermo Fisher). An Affymetrix GeneChip Fluidics Station was used to perform streptavidin/phycoerythrin staining. The hybridization signals on the microarray were scanned using

a GeneChip Scanner 3000 (Thermo Fisher) and array data analysis was performed with Expression console software 1.2 (Thermo Fisher). Normalization was performed with MAS5 algorithm using a set of mouse maintenance genes (Thermo Fisher). Data was provided by Dr. Y. Sato and Dr. T. Kuroda (National Institute of Health Sciences).

Western blot

Frozen heart samples were harvested in lysis buffer containing (in mM) 120 NaCl, 20 Tris-HCl, 1%(v/v) TritonX-100, 0.1% SDS, 0.5% sodium deoxycholate, 10% glycerol, 1 EDTA (pH 7.4) and protease inhibitor cocktail (Nacalai). Cell lysates were sonicated and clarified by centrifugation for 10 min (at 10,000 xg) at 4°C. The supernatants were equalized for amount of protein (DC^{TM} protein assay, BIORAD) and suspended in SDS sample buffer containing 0.1 M DTT, following incubation for over 1 h at room temperature. Protein samples were fractionated by SDS-PAGE and transferred onto PVDF membranes (Millipore). The desired proteins were then detected using the indicated primary antibodies overnight at 4°C. After incubation with secondary antibodies, immunoreactive bands were detected using Western Lightning Plus ECL (PerkinElmer) and images were captured with an ImageQuant LAS 4000 (GE healthcare Life Science).

Bioluminescence resonance energy transfer (BRET)

HEK293 cells were transfected with β_1AR-Rluc, βArr2-YFP (energy acceptor), along with mCherry vector, TRPC6(WT)-mCherry, TRPC3(WT)-mCherry, or TRPC6(DN)-mCherry. 48 h after transfection, cells were detached with PBS/EDTA (2 mM) and centrifuged for 5 min (1000 xg, at room temperature). After centrifugation, cell pellets were resuspended in BRET buffer (1.8 mM $CaCl_2$, 1 mM $MgCl_2$, 0.1% glucose in PBS) and removed to 96-well white microplate. The cells were stimulated with ISO (10 μM) for 30 min and incubated with coelenterazine h (5 μM, Wako) for 10 min. Readings

were collected by a fluorescent microplate reader (SpectraMax® i3, Molecular devices). The BRET signal was determined as the ratio of the light emitted by YFP and the light emitted by Luc. The values were corrected by subtracting the background BRET signals. The ΔBRET defined as ISO-stimulated – non-stimulated BRET ratio.

Statistical analysis

All results were presented as the mean ± SEM from at least 3 independent experiments. Statistical comparisons were carried out by unpaired t tests for two-group comparisons or one-way analysis of variance (ANOVA) followed by Tukey's *post hoc* test for multiple groups. Values of $P<0.05$ were considered to be statistically significant.

Results

<Chapter 1>

TRPC6 positively regulates cardiac inotropy by enhancing β adrenergic receptor signaling

Deletion of TRPC6 reduced a positive inotropic effect after βAR stimulation

First, I investigated cardiac responses through autonomic nervous system by activating each responsible receptor. In association with an injection of ISO (non-selective βAR agonist; 10 pg/g/min) intravenously, cardiac contractility (shown as dP/dt_{max}) and heart rate were increased in wild type (WT) mice (Fig.1A, B). However, a positive inotropic effect was significantly reduced in TRPC6-deficient mice, whereas there was little difference between WT and $TRPC6^{(-/-)}$ mice in a positive chronotropic effect. TRPC3-deficient mice showed both ISO-induced positive inotropic and chronotropic effects. After injection of ACh (0.5 mg/kg), all groups showed decreases of cardiac contractility and heart rate to a similar extent (Fig.1C). NE (0.05 mg/kg) administration caused the transient increases of systolic/diastolic blood pressure in WT, TRPC3 and TRPC6-deficient mice (Fig.1D). These results suggest that TRPC6, but not its closest homolog TRPC3, is involved in regulation of cardiac contractility following βAR activation.

TRPC6 exists in close proximity to βAR in left ventricle

Next, I investigated the reason why only a positive inotropic effect was reduced in TRPC6-deficient mice. Heart is composed of various kinds of cell types (e.g. cardiomyocyte, fibroblast, smooth muscle cell) and each cell type has unique characteristics. Ventricular cardiomyocytes contribute to regulation of cardiac contractility, and pacemaker cells of the sinoatrial node (SAN) determine heart rate. I compared the localization of TRPC6 and βAR proteins between left ventricle and SAN. I identified

SAN cells by immunostaining potassium/sodium hyperpolarization-activated cyclic nucleotide-gated channel 4 (HCN4) specifically expressed in SAN (Fig.2A, B). The TRPC6 distribution was verified by proximity ligation assay (PLA) between endogenous TRPC6 and β_1AR. In PLA, two different proteins in close proximity (at distances <40 nm) are detected as puncta using a pair of oligonucleotide-labeled antibodies and enzymatic reaction. The number of PLA puncta was significantly larger in LV cardiomyocytes than that in SAN cells (Fig.2C, D). In addition, TRPC6-β_1AR PLA signals were observed in isolated cardiomyocytes; that is, TRPC6 interacted with β_1AR in ventricular cardiomyocytes (Fig.3A). TRPC6-β_1AR PLA signals existed at basal states and the number of signals does not change even though cells were stimulated with ISO (10 nM) for 30 or 60 min (Fig.3B). There was no significant difference in βAR expression between WT and TRPC6$^{(-/-)}$ mice at the protein levels (Fig.4A) and mRNA levels (Fig.4B). Taken together, it is suggested that TRPC6 exists in close proximity to β_1AR in LV cardiomyocyte.

TRPC6 regulates βAR-Gs signaling and cardiomyocyte contraction

Based on the results in Fig.1-4, I hypothesized that TRPC6-β_1AR interaction in ventricular cardiomyocytes was involved in ISO-stimulated regulation of cardiac contraction. To test this hypothesis, I investigated whether deletion of TRPC6 altered cardiomyocyte contractility in primary isolated adult mice cardiomyocytes. Sarcomere (the structural unit in striated muscle tissue) length shortening of single cardiomyocyte was measured with electrically pacing (4 Hz). Consistent with the results of cardiac catheterization, the increase in sarcomere length shortening amplitude following ISO treatment (10 nM) was reduced in cardiomyocytes from TRPC6-deficient mice (Fig.5A, B. These data were provided by Dr. Y. Yamaguchi and Prof. G. Iribe in Asahikawa medical university). Cardiomyocyte contraction is triggered by changes in intracellular Ca^{2+} concentration after evoking an action potential (E-C coupling). I measured Ca^{2+} transient after ISO exposure in field-stimulated (1

Hz) cardiomyocyte from WT and TRPC6$^{(-/-)}$ mice. In support of Fig.5A and B, increase in Ca^{2+} transient amplitude following ISO stimulation (10 nM) was reduced in cardiomyocytes from TRPC6-deficient mice (Fig.5C, D). β_1AR couples to Gs and increases intracellular cyclic adenosine monophosphate (cAMP) production after receptor activation. To investigate whether TRPC6 affected cAMP production, I used Epac-based FRET biosensor detecting cAMP. This biosensor was designed based on Epac (exchange protein directly activated by cAMP), which is activated directly by cAMP, sandwiching between cyan fluorescent protein (CFP) and yellow fluorescent protein (YFP) (gifted by Prof. K. Jalink in the Netherlands Cancer Institute) [30]. Once cAMP binds to Epac, a conformational change in Epac occur and förster resonance energy transfer (FRET) between CYP and YFP reflects this change. Neonatal rat cardiomyocytes (NRCMs) were transfected with Epac-based FRET biosensor and stimulated with ISO (1 μM). βAR activation-dependent increase of intracellular cAMP production was reduced in TRPC6-silenced NRCMs (Fig.5E-G). Contrary to reduction of Ca^{2+} transient amplitude in cardiomyocytes from TRPC6-deficient mice, mRNA expression of various factors related to intracellular calcium regulation tended to increase in TRPC6-deficient mouse hearts and some was significantly increased (Fig.6A). In addition, there was no significant change in mRNA expression of enzymes for cAMP conversion and G proteins among TRPC6-silencing NRCMs or WT, TRPC6$^{(-/-)}$ and TRPC3$^{(-/-)}$ mouse hearts (Fig.6B, C). Therefore, it is suggested that TRPC6 is a positive regulator of βAR-Gs signaling, contributing to cardiac positive inotropy in ventricular cardiomyocytes.

TRPC6-deficient cardiomyocyte contains lower level of intracellular zinc

The above results revealed that TRPC6 was involved in regulation of βAR signaling in cardiomyocyte. However, TRPC3, which was very similar to TRPC6 functionally and structurally, did not participate in βAR signaling regulation. To clarify a detailed mechanism of regulation of βAR via TRPC6, I focused on this difference between TRPC6 and TRPC3. Since TRPC6 is non-selective cation

channel, it permeates various cation not only Ca^{2+} and Na^{+} which play important roles in maintaining intracellular homeostasis. TRPC6, but not TRPC3, can permeate zinc ion (Zn^{2+}). As previously reported, HEK293 cell expressing TRPC6 stably allowed Zn^{2+} entry and had a larger intracellular pool of Zn^{2+} [32]. In terms of relation between Zn^{2+} and βAR signaling, it has been reported that Zn^{2+} enhanced agonist affinity and intracellular cAMP accumulation by modulating β_2AR allosterically [33]. While Zn^{2+} is a possible factor involved in regulation of βAR signaling by TRPC6, studies about functions of Zn^{2+} in the heart are still limited. I therefore analyzed accumulation of intracellular Zn^{2+} in ventricle cardiomyocytes isolated from WT, TRPC6$^{(-/-)}$ and TRPC3$^{(-/-)}$ mice. To assess intracellular Zn^{2+} store, cardiomyocytes were loaded with FluoZin-3, a Zn^{2+}-selective indicator and monitored change in fluorescence intensity after treatment with the oxidant, 2,2′-dithiodipyridine (DTDP, 100 μM). DTDP oxidizes intracellular protein and causes Zn^{2+} release from intracellular Zn^{2+} pool [34]. Cardiomyocytes from TRPC6-deficient mice showed lower FluoZin-3 fluorescent signals after treatment of DTDP compared to cardiomyocytes from WT and TRPC3-deficient mice (Fig.7A, B). There was no significant difference with the mRNA expression levels of zinc transporters, ZIPs (increase cytoplasmic zinc level by zinc import) and ZnTs (decrease cytoplasmic zinc level by zinc export), and metallothioneins (MTs, metal-binding protein) (Fig.7C). Therefore, TRPC6 is involved in regulation of intracellular Zn^{2+} dynamics in cardiomyocyte.

αAR-TRPC6-Zn^{2+} axis enhances βAR-Gs signaling

To regulate intracellular Zn^{2+} dynamics through TRPC6 which activates via ligand-mediated receptor activation, it is necessary that Gq-coupled receptor is located on the upstream of TRPC6. I focused on αAR as a promising candidate for the following reasons: 1) αAR is activated by NE released from sympathetic nerve endings. 2) αAR is present in the heart [35]. 3) Several studies have reported that αAR interacts with TRPC6 and increases TRPC6 activity by αAR stimulation [36,37].

Although both αAR and βAR are expressed in the heart, the expression level of αAR is much lower than βAR (α:β=1:9)[2]. In addition, βAR inhibitor significantly suppressed ligand (NE, ISO and adrenaline)-mediated contraction of human cardiomyocyte [38]. Hence, it is generally believed that βAR mainly contributes to regulation of cardiac function. However, ligand affinity of NE, physiological ligand, to βAR is only 5% compared to ISO, artificial ligand [39]. Furthermore, previous study has demonstrated that NE with a concentration over 10 times higher than ISO is necessary to induce contraction in human papillary cardiomyocyte equivalent to that induced by ISO stimulation [38]. In fact, NE binds to αAR preferentially compared to βAR in human [40]. Thus, it is still incompletely understood how βAR signaling is regulated by NE even if ligand affinity and response to NE are not high. Considering previous studies, I hypothesized as follows: αAR activated by NE operates TRPC6, which increase in intracellular Zn^{2+} concentration and this increase of Zn^{2+} enhances βAR-Gs signaling pathway. To test this hypothesis, I began with investigating whether TRPC6 permeated Zn^{2+} in the downstream of αAR. HEK293 cells expressed with vector, TRPC6 or TRPC3 along with α_{1A}AR were assessed change of FluoZin-3 fluorescence intensity after NE stimulation. Since a previous report have shown that TRPC6 interacts with α_{1A}AR in cardiomyocytes [41], I used α_{1A} subtype for transfection. After NE stimulation (10 μM) with extracellular Zn^{2+}, only TRPC6-expressing HEK cells showed NE-mediated Zn^{2+} influx (Fig.8A, B). As previously reported [32], gradual increases of FluoZin-3 fluorescence after application of extracellular Zn^{2+} were observed in each group, indicating that universal entry of Zn^{2+} exists in HEK cells. I confirmed that TRPC6 were activated in the downstream of Gq-coupling α_{1A}AR, not Gs-coupling β_1AR by Ca^{2+} imaging (Fig.8C, D). Next, I investigated whether intracellular Zn^{2+} dynamics affected βAR signaling pathway. Firstly, NRCMs were treated with prazosin (α_1AR inhibitor), propranolol (βAR inhibitor) and N,N,N',N'-Tetrakis(2-pyridylmethyl)ethylenediamine (TPEN, Zn^{2+} chelator) and measured intracellular cAMP production after NE stimulation. The increase in cAMP production following NE stimulation (1 μM) was

significantly suppressed by αAR inhibition and intracellular Zn^{2+} chelation (Fig.8E). βAR inhibition completely reduced cAMP production. Second, NRCMs were treated with methoxamine (αAR agonist) in Zn^{2+}-containing medium for 1 day and stimulated by ISO (1 μM). In this experiment, cells were primed with Zn^{2+} by activation of α_AAR-TRPC6 pathway. αAR activation enhanced cAMP production by ISO stimulation (Fig.8F). In contrast, this enhancement was cancelled in siTRPC6-treated cells (Fig.8G). These results suggest that Zn^{2+} influx via TRPC6 is necessary for enhancement of cAMP production with αAR activation, and that αAR-TRPC6-Zn^{2+} axis is involved in modulation of βAR-Gs signaling pathway in cardiomyocyte.

TRPC6 is involved in physiological regulation of cardiac contractility

As shown in Fig.1, I have used ISO to show that a positive inotropic effect was reduced in TRPC6-deficient mice. However, under physiological conditions, endogenous βAR ligand is NE, released from sympathetic nerve endings. To analyze a physiological inotropic effect, baroreflex, one of the physiological reflex responses, was induced in mice. Baroreflex is a homeostatic mechanism to keep blood pressure constant; baroreceptors in the carotid sinus and the aortic arch sense fluctuations of blood pressure and transmit signals to brainstem, which triggers modulation of autonomic nervous system and buffering blood pressure change [42,43]. For instance, when baroreceptors detect decrease in blood pressure, the sympathetic nervous system is activated, followed by increased level of NE released at nerve endings in the heart, resulting in induction of a positive inotropic effect and chronotropic effect. The baroreflex response was evoked by hydralazine in mice and following inotropic effect and chronotropic effect were measured by cardiac catheterization. Hydralazine induces vasodilation and decrease in blood pressure by acting on vascular smooth muscle directly. This compound reportedly elicits compensatory activation of sympathetic nervous system and NE release in mouse and human [44]. A positive inotropic effect induced by hydralazine injection (0.5 mg/kg) was

significantly reduced in TRPC6-deficient mice (Fig.9A). On the other hand, there was no significant difference in a chronotropic effect between WT and TRPC6$^{(-/-)}$ mice (Fig.9B). In addition, gradual decrease in systolic and diastolic blood pressure by transient hydralazine injection did not differ markedly between WT and TRPC6$^{(-/-)}$ mice (Fig.9C). Thus, these results suggest that TRPC6 is involved in physiological regulation of cardiac contractility.

Hyperglycemia-induced TRPC6 upregulation enhances baroreflex-dependent cardiac contraction.

Finally, I examined whether a positive inotropic effect is enhanced by TRPC6 upregulation in the heart. I previously reported that hyperglycemia increases TRPC6 expression level in the heart [22]. Based on this study, reflex inotropic effect was assessed in mice which developed streptozotocin (STZ)-induced hyperglycemia. STZ (50 mg/kg), which has selective toxicity to pancreatic beta cells, was injected to mice intraperitoneally for consecutive five days. Blood glucose levels were significantly increased 4 weeks after final injection (Fig.10A). A positive inotropic effect was enhanced in STZ-injected mice (Fig.10B), while a chronotropic effect did not differ significantly between STZ(-) and STZ(+) group (Fig.10C). At the base of heart, TRPC6-β_1AR PLA signals were increased in STZ-injected mice (Fig.10D, E). In contrast, there was no significant difference in PLA signals at the apex region. According to these results, hyperglycemia-induced TRPC6 upregulation enhances baroreflex-dependent cardiac contraction.

<Chapter 2>

TRPC6 is involved in ligand-stimulated β_1AR internalization process

Multiple intracellular signals pathway related to βAR

Once βAR is activated by ligand binding, a series of downstream components transmits the signal into cells and the signal transduction cascade changes over time [45]. First, activation of Gαs subunit triggers activation of adenylate cyclase and following cAMP production. Increase of intracellular cAMP concentration leads to activation of protein kinase A, resulting in phosphorylation of various intracellular effectors and subsequent cellular responses. To keep a balance between receptor activation and signaling amplitude, negative feedback loop signal is induced: receptor desensitization and internalization processes that lead to termination of the signaling cascade. Ligand-occupied receptor is phosphorylated by G protein-coupled receptor kinase (GRK) and β-arrestin (βArr) is recruited to the phosphorylated receptor, leading to receptor internalization through clathrin-mediated endocytosis. In Chapter 2, I investigated an involvement of TRPC6 in βAR internalization process.

TRPC6 suppressed ligand-induced receptor internalization and βArr2 translocation

GFP-tagged β_1AR and mCherry-tagged TRPC6 or TRPC3 were co-expressed in HEK293 cells and receptor internalization was induced by 30-min ISO stimulation (10 μM). Receptor internalization was observed by ISO-dependent redistribution of GFP signals into intracellular space (Fig.11A). Compared to vector-expressed cells, receptor internalization was suppressed in TRPC6-expressed cells (Fig.11B). On the other hand, pore-dead dominant negative mutant of TRPC6 (TRPC6-DN, with LFW motif deleted) and TRPC3 did not suppress receptor internalization. Next, I assessed ligand-mediated membrane translocation of βArr2. YFP-tagged βArr2, β_1AR and TRPC6 or 3 were co-expressed in HEK293 cells. In vector-expressed cells, βArr2 translocated from the cytoplasm to cell membrane

after ISO stimulation (Fig.11C). Associated with the results of receptor internalization, translocation of βArr2 was suppressed in TRPC6-expressed cells (Fig.11D). In addition, TRPC6-DN and TRPC3 did not affect βArr2 translocation. Membrane translocation of βArr2 was also assessed by bioluminescence resonance energy transfer (BRET). Interaction between β_1AR and βArr2 following ISO stimulation was decreased markedly in TRPC6-overexpressed HEK293 cells (Fig.11E). In contrast, TRPC6-DN and TRPC3 did not reduce the interaction. These results suggest that TRPC6 suppresses membrane translocation of βArr2 and following β_1AR internalization in HEK cells. In primary adult mice cardiomyocytes, interaction between β_1AR and βArr2 at the basal level, shown as the number of PLA puncta, was significantly reduced in cells from TRPC6-deficient mice (Fig.12A, B). The mRNA expression of βArr2 in WT and TRPC6$^{(-/-)}$ mice and protein expressions of GRK2/5/6 in WT, TRPC6$^{(-/-)}$, TRPC3$^{(-/-)}$ and TRPC3/6$^{(-/-)}$ mice were not significantly different (Fig.12 C, D). Based on these results, TRPC6 is involved in ligand-stimulated βAR internalization process.

<Chapter 3>

Involvement of TRPC6 in isoproterenol-induced heart failure

Chronic βAR activation and heart failure

In Chapter 1 and 2, I have assessed acute βAR responses evoked in several seconds to tens of minutes after ligand stimulation. On the other hand, a chronic enhancement of βAR signaling is highly involved in pathogenesis of heart failure. During the development and progression of heart failure, sympathetic nervous system is accelerated, leading to increase in systemic adrenergic responses. This is due to compensation of lowered cardiac performance. However, continuous βAR stimulation causes βAR downregulation and uncoupling of Gs protein, resulting in exacerbation of heart failure [46]. I therefore investigated whether TRPC6 is involved in the progression of cardiac remodeling caused by chronic βAR activation.

TRPC6 is involved in modulation of a chronic βAR signaling

WT, TRPC6$^{(-/-)}$, TRPC3$^{(-/-)}$ and TRPC3/6$^{(-/-)}$ mice were continuously treated with ISO (30 mg/kg) subcutaneously using osmotic pump. After 4 weeks, water intake, food intake (Fig.13A) and the amount of total cholesterol in plasma (Table.3) were increased, and the amounts of triglyceride and glucose were decreased. While feeding behavior and energy metabolism were changed by βAR stimulation in the whole body, there is no significant difference among each group. Chronic ISO treatment did not damage kidney, liver and muscle tissue according to values of blood urea nitrogen (BUN), alanine aminotransferase (ALT)/ aspartate aminotransferase (AST) and creatine phosphokinase (CPK) respectively (Table.3). The rectal temperature was not affected by ISO treatment and mouse strain (Fig.13B). Chronic βAR stimulation induced decrease in fractional shortening (FS) and increase in LV internal dimension in systole (LVIDs) in WT and TRPC3$^{(-/-)}$ mice (Fig.13C, D,

Table.4). FS is an indicator of cardiac contractility and increase in LVIDs means that cardiac contraction is reduced. These data suggest that cardiac function was lowered in WT and TRPC3$^{(-/-)}$ mice by chronic ISO treatment. In contrast, changes in these indices were canceled in TRPC6$^{(-/-)}$ and TRPC3/6$^{(-/-)}$ mice. In addition, max LV pressure was increased in TRPC6-deficient mice with ISO treatment (Table.5). ISO administration increased the ratios of heart weight to body weight (BW) in each mouse strain, and this change was enhanced in TRPC6-deficient mice compared to WT mice (Fig.13E). Although the average size of ventricular cardiomyocytes was markedly increased by ISO administration, the levels of hypertrophy were not different between WT and TRPC6$^{(-/-)}$ mice (Fig.13F, G). The mRNA expression level of TRPC6 in the heart was increased significantly 4-week after ISO administration, whereas the mRNA level of TRPC3 was not significantly changed (Fig.13H). The ISO-induced increases in weight (ratio to BW) of some skeletal muscles, where β_2AR is highly expressed, were also enhanced in TRPC6-deficient mice, indicating that TRPC6 may negatively regulate ISO-induced striated muscle tissue remodeling in mice (Table.6). These results suggest that TRPC6 participates in βAR-mediated cardiac inotropy and chronic striated muscle tissue remodeling in mice.

Discussion

In this research, I aimed to reveal physiological roles of TRPC6 focusing on adaptive changes in cardiac functions regulated by autonomic nervous system. First, I found that ISO-induced positive inotropic effect was reduced in TRPC6-deficient mice, whereas there was no significant difference in a chronotropic effect between WT and TRPC6$^{(-/-)}$ mice (Fig.1). TRPC6 exists in close proximity to β_1AR in LV cardiomyocytes, but not SAN cells (Fig.2, 3). Consistent with Fig.1, ISO-induced increase in sarcomere length shortening and Ca^{2+} transient was reduced in LV cardiomyocytes from TRPC6-deficient mice (Fig.5A-D). βAR activation-dependent increase of intracellular cAMP production was reduced in TRPC6-silenced NRCMs (Fig.5E-G). These results suggest that TRPC6 is a positive regulator of βAR-Gs signaling, contributing to cardiac positive inotropy in response to sympathetic nerve stimulation. To reveal the mechanism underlying enhancement of βAR-Gs signaling by TRPC6, I focused on αAR-mediated Zn^{2+} influx through TRPC6 and found the following: 1) Intracellular Zn^{2+} pool in TRPC6-deficient cardiomyocytes was smaller compared to WT and TRPC3$^{(-/-)}$ mice (Fig.7). 2) TRPC6 permeates Zn^{2+} in response to α_{1A}AR stimulation (Fig.8A, B). 3) αAR inhibition and chelation of intracellular Zn^{2+} suppressed NE-induced cAMP production (Fig.8E). 4) TRPC6 activation, mediated by αAR stimulation, enhanced ISO-induced cAMP production, and this enhanced cAMP production was canceled by TRPC6 gene-silencing (Fig.8F, G). A reflex inotropy as physiological response was reduced in TRPC6-deficient mouse hearts (Fig.9). In addition, hyperglycemia-induced TRPC6 upregulation enhances baroreflex-dependent positive inotropy (Fig.10). In Chapter 1, I revealed that TRPC6 positively regulates cardiac contractility by enhancing βAR-Gs signaling through αAR-Zn^{2+} axis (Fig.14). In Chapter 2, I investigated the involvement of TRPC6 in βAR internalization process. TRPC6 suppressed ISO-induced βAR internalization and βArr2 translocation in HEK293 cell (Fig.11). Interaction between β_1AR and βArr2 at the basal level

was reduced in TRPC6-deficient cardiomyocytes (Fig.12). These results suggest that TRPC6 is involved in ligand-stimulated βAR internalization process. In chapter 3, I examined whether TRPC6 is involved in the progression of cardiac remodeling by chronic βAR activation. ISO-induced cardiac dysfunction (shown as decrease in FS and increase in LVIDs) was cancelled in TRPC6-deficient mice (Fig.13C, D). ISO-mediated increase in heart weight were enhanced in TRPC6$^{(-/-)}$ mice (Fig.13E). The mRNA expression level of TRPC6 was increased after chronic βAR activation (Fig.13H). These results suggest that TRPC6 participates in βAR-mediated cardiac positive inotropy and chronic remodeling of heart in mice.

TRPC6-mediated Zn^{2+} influx enhances βAR-Gs signaling

Zinc (Zn) is the secondary abundant trace metal after iron in human and involved in various physiological processes: cell division, growth, immune response, hormone metabolism, and reproduction. Zn binds to ~10% of all proteins encoded in the human genome [47], and contribute to maintenance of protein structure and modulation of enzymatic activities. Some DNA-binding proteins such as transcription factors interact with DNA through Zn-binding domain (e.g., zinc finger, LIF motif, RING finger). Extracellular and intracellular Zn concentrations are 10-1000 μM and 10-100 μM respectively [48]. However, almost all intracellular Zn bind to proteins or distribute in organelles and vesicles, and therefore the actual intracellular Zn^{2+} concentration in the cytosol (free Zn^{2+}) is quite low (pM to low μM) [49]. Zn^{2+} does not have redox reactivity unlike iron ion and copper ion, resulting in low toxicity to cells in the form of labile Zn^{2+}. Previous reports have shown that labile Zn^{2+} functions as a second messenger in association with increase in intracellular Zn^{2+} concentration [50]. Based on these features, Zn is considered as “the calcium of the 21 centuries” [51]. Although some studies have reported that Zn^{2+} dynamics is related to the regulation of cardiac functions and pathology of cardiovascular diseases [52], physiological functions of Zn^{2+} in cardiomyocytes and regulatory

mechanisms are still unclear. In this research, I found out a new role of local Zn^{2+} in cardiomyocytes: αAR-triggered Zn^{2+} influx, mediated by TRPC6, enhances βAR-Gs signaling.

Although it is generally accepted that Zn^{2+} dynamics is regulated by Zn transporters, several reports and this study showed that ion channels are also involved in Zn^{2+} regulation. There are two characteristics in Zn^{2+} regulation by channels: 1) channels can permeate ions faster (~10^8 ions/s) than transporters (10^2-10^5 molecules/s) [53]. 2) ROCCs such as TRPC6 open by specific stimulation. According to these characteristics, channels are capable of regulating intracellular Zn^{2+} dynamics in a spaciotemporal manner. Even though mRNA expression levels of zinc transporters and metallothioneins did not differ significantly between WT and TRPC6-deficient mice (Fig.7C), I have not verified whether zinc transporters are involved in TRPC6-mediated Zn^{2+} mobilization. Further studies about the functional relationship between TRPC6 and zinc transporters are required to understand local Zn^{2+} dynamics in cardiomyocytes comprehensively through sympathetic nerve activation.

Specific alignments of TRPC6 for Zn^{2+} permeability have not identified yet. In addition to TRPC6, some TRPs are reportedly permeates Zn^{2+}: TRPM3/6/7, TRPA1, TRPV6 and TRPML1 [54]. Previous study has shown that Asp 915 in TRPA1 channel pore region is involved in Zn^{2+} entry [55]. Furthermore, Glu1047 and Glu1052 in pore domain of TRPM7 (Glu1024 and Glu1029 are corresponding residues in TRPM6) play an important role in Zn^{2+} permeability [56]. Therefore, acidic amino acid residues in channel pore region are assumed to determine Zn^{2+} permeability. In comparison of amino acid sequences among TRPC6 and other Zn^{2+} permeable TRPs, there is no acidic amino acid residue conserved in the corresponding position of TRPC6. Among TRPC6, TRPC3 and TRPC7 (close homolog of TRPC3 and 6), TRPC6 contains some different amino acid residues from TRPC3/7 in pore region. I am proceeding with further investigation about Zn^{2+} permeability of TRPC6 using mutants in which several amino acid residues in TRPC6 pore domain are replaced to that of TRPC3. The above

amino acid residues for Zn^{2+} permeability is involved in not only Zn^{2+} entry but also other divalent cations. To investigate specific mechanisms for Zn^{2+} entry, it is necessary to verify structure and function of TRPC6 from other aspects such as three-dimensional (3D) structure.

There are two possibilities considered how Zn^{2+} enhances βAR-Gs signaling in LV cardiomyocytes. One is that Zn^{2+} interact with βAR directly and contributes to conformational change. Previous study has reported that Zn^{2+} binding to β_2AR enhances ligand affinity and accumulation of intracellular cAMP [33]. Further research has shown that Zn^{2+} binds to His269, Cys265 and Glu225 in cytoplasmic region of human β_2AR and bridge between transmembrane domain 5 and 6, leading to increase in ligand affinity [57]. Although these three residues are not conserved completely in human β_1AR, other residues which have similar characteristics are positioned. The other is that Zn^{2+} enhances βAR-Gs protein interaction. According to 3D simulation done by Prof. S. Kiyonaka (Nagoya university), it is predicted that Zn^{2+} intervenes between βAR and Gs protein through three amino acid residues in βAR-Gs interaction site, resulting in enhancement of βAR-Gs interaction. To investigate these possibilities, I plan to construct βAR and Gs mutants whose Zn^{2+}-sensitive residues were substituted and analyze the impact on cardiac positive inotropy induced by sympathetic nerve stimulation.

Relation between increase in TRPC6 expression and hyperactivation of βAR-Gs signaling

I showed that hyperglycemia-induced TRPC6 upregulation and increase in TRPC6-βAR interaction enhanced baroreflex-induced positive inotropic effect in the heart (Fig.10). Thus, increase in TRPC6 expression in the heart is considered to enhance βAR responsiveness to physiological ligand NE and subsequent enhancement of cardiac contraction. Since prolonged hyperactivation of βAR-Gs signaling is detrimental to the heart [58], increase of TRPC6 expression in the heart may lead to cardiac dysfunction through hyperactivation of βAR-Gs signaling. Indeed, the mRNA expression level of TRPC6 was increased in hearts whose function was decreased by chronic ISO injection (Fig.13H). ISO-induced

cardiac dysfunction was suppressed in TRPC6-deficient mice (Fig.13C, D). In addition, TRPC6 is upregulated in human failing hearts [18,19]. Therefore, the expression level of TRPC6 is considered to be highly associated with βAR reactivity to NE.

Takotsubo syndrome (stress-induced cardiomyopathy) is thought to be triggered by increased sympathetic nerve activity and catecholamine spillover [59,60]. Previous studies have shown that this syndrome is preceded by strong physiological stress or emotional stress [61]. In fact, cases of Takotsubo syndrome were increased after Mid Niigata Prefecture Earthquake in 2004 [62]. This syndrome is characterized by sudden and transient contractile dysfunction in the LV apex region (expressed as "transient apical ballooning") and hypercontraction in the base region. Although patients recover from above symptoms within weeks to months, long-term prognosis is not well; morbidity rate of cardiovascular events was 9.9% (per patient per year) and mortality rate was 5.6% (per patient per year) [63]. However, pathogenesis has not been well understood and effective treatment has not established. One possible mechanism of transient apical dysfunction is an alteration of intracellular homeostasis in cardiomyocytes; hyperactivation of βAR-Gs signaling by catecholamine spillover leads to hypercontraction, which induces imbalance of cell responses such as hypoxia, deposition of lipid droplets, mitochondrial dysfunction and cationic imbalance, resulting in apical dysfunction [64]. Increase of TRPC6 expression in cardiomyocytes might be contributed to this hypercontraction through enhancement of βAR-Gs signaling. Since approximately 90% patients are menopausal female [61], TRPC6 could be upregulated in their hearts. In addition, it is speculated that distributions of TRPC6 and βAR are associated with difference of contractile phenotype between the apex and the base in Takotsubo syndrome. Thus, evaluation of βAR regulation via TRPC6 in terms of age, sex and distribution of TRPC6 and βAR in the heart might give new insights into pathology of Takotsubo syndrome.

Involvement of TRPC6 in βAR internalization

I found that ISO-induced β_1AR internalization and βArr2 translocation are suppressed in TRPC6-coexpressed HEK cells (Fig.11). On the other hand, β_1AR interacted with βArr2 in LV cardiomyocytes under the resting condition and this interaction was reduced in that of TRPC6-deficient cardiomyocytes (Fig.12). The contradiction between these results is considered to be due to following reasons: 1) Expression levels of TRPC6, βAR and βArr2 and the expression ratio among these proteins are different between artificial (overexpression system in HEK cells) and physiological condition. 2) Endogenous catecholamine stimulates βAR and might repeat receptor activation-inactivation cycles constantly in physiological condition. This is one of possible reasons why PLA puncta between β_1AR and βArr2 were observed at the basal level. Although overexpression system is widely accepted strategy for evaluating receptor internalization, the results might not correspond to that of physiological condition. Since βArr2 translocation is triggered by preceding Gs signaling and receptor phosphorylation process [65], decrease of β_1AR-βArr2 interaction in TRPC6$^{(-/-)}$ cardiomyocytes seems to be due to reduction of Gs signaling. Further studies such as phosphorylation of receptor and related factors are required.

The role of TRPC6 in the pathogenesis of heart failure

I found LV dysfunction induced by chronic ISO injection is suppressed in TRPC6-deficient mice (Fig.13C, D). In addition, the mRNA expression level of TRPC6 was increased in hearts whose function was impaired by chronic βAR stimulation (Fig.13H). TRPC6 is considered to enhance βAR-Gs signaling chronically, resulting in aggravation of LV dysfunction and upregulated owing to compensation of impaired function. Although I first expected that ISO-induced increase in heart weight is also suppressed in TRPC6-deficient mice, the result was opposite: increase in heart weight was enhanced in TRPC6-deficient mice compared to WT (Fig.13E). These results suggest that

regulatory mechanisms of LV function and cardiac hypertrophy are different in the pathogenesis of heart failure caused by chronic βAR stimulation. Indeed, ISO-induced LV dysfunction was ameliorated in TRPC3/6 double knockout mice, while aggravation of increase in heart weight was not observed. Physiological LV function may be positively regulated by TRPC6, whereas both TRPC3 and TRPC6 channels seem to be involved in the induction of cardiac hypertrophy. Cardiac remodeling is mediated by not only cardiomyocytes but also other types of cells such as fibroblasts and macrophages. The extents of ISO-induced cardiomyocyte hypertrophy were not different between WT and TRPC6$^{(-/-)}$ mice (Fig.13F, G). In addition, since I used systemic knockout mice, every cell lacks TRPC3 or TRPC6 gene. Therefore, further study is required to determine the contribution of non-cardiomyocytes to ISO-induced cardiac remodeling.

βAR signaling regulates not only cardiac function but also other biological responses: relaxation of smooth muscle cells [66], thermogenesis and energy metabolism in brown adipose tissue [67] and regulation of mass and glucose metabolism in skeletal muscle [68,69]. Since the weight of some skeletal muscles was significantly increased in TRPC6-deficient mice compared to WT (Table.6), TRPC6 might be involved in the enhancement of βAR signaling in other muscular organs. By clarifying the role of TRPC6 in β-receptor signaling in skeletal muscle, it will be able to show the universality of my new concept elucidated in this study.

Future perspective

Collectively, I revealed that TRPC6 links between αAR signaling and βAR signaling through Zn^{2+} mobilization, leading to enhancement of cardiac positive inotropy in response to sympathetic nerve activation. Furthermore, I found that TRPC6 regulates Zn^{2+} dynamics in cardiomyocyte and Zn^{2+} is involved in regulation of inotropy. This regulation possibly contributes to pathogenesis of heart failure based on this research, and therefore further study about αAR-TRPC6-βAR pathway might clarify

pathology of heart diseases. In addition, since TRPC6 is expressed universally and various biological responses are regulated by sympathetic nervous system, Zn^{2+}-dependent enhancement of βAR signaling via TRPC6 might be involved in other physiological responses.

References

1 Gordan, R., Gwathmey, J. K. & Xie, L. H. Autonomic and endocrine control of cardiovascular function. *World J Cardiol* **7**, 204-214, doi:10.4330/wjc.v7.i4.204 (2015).

2 O'Connell, T. D., Jensen, B. C., Baker, A. J. & Simpson, P. C. Cardiac alpha1-adrenergic receptors: novel aspects of expression, signaling mechanisms, physiologic function, and clinical importance. *Pharmacol Rev* **66**, 308-333, doi:10.1124/pr.112.007203 (2014).

3 J, O. U. *et al.* Interaction of alpha1-adrenoceptor subtypes with different G proteins induces opposite effects on cardiac L-type Ca^{2+} channel. *Circ Res* **102**, 1378-1388, doi:10.1161/CIRCRESAHA.107.167734 (2008).

4 Chu, C. *et al.* Intraventricular and interventricular cellular heterogeneity of inotropic responses to alpha(1)-adrenergic stimulation. *Am J Physiol Heart Circ Physiol* **304**, H946-953, doi:10.1152/ajpheart.00822.2012 (2013).

5 Landzberg, J. S., Parker, J. D., Gauthier, D. F. & Colucci, W. S. Effects of myocardial alpha 1-adrenergic receptor stimulation and blockade on contractility in humans. *Circulation* **84**, 1608-1614, doi:10.1161/01.cir.84.4.1608 (1991).

6 Hofmann, T., Schaefer, M., Schultz, G. & Gudermann, T. Transient receptor potential channels as molecular substrates of receptor-mediated cation entry. *J Mol Med (Berl)* **78**, 14-25, doi:10.1007/s001099900070 (2000).

7 Montell, C. & Rubin, G. M. Molecular characterization of the Drosophila trp locus: a putative integral membrane protein required for phototransduction. *Neuron* **2**, 1313-1323, doi:10.1016/0896-6273(89)90069-x (1989).

8 Clapham, D. E. TRP channels as cellular sensors. *Nature* **426**, 517-524, doi:10.1038/nature02196 (2003).

9 Kiselyov, K., Kim, J. Y., Zeng, W. & Muallem, S. Protein-protein interaction and functionTRPC channels. *Pflugers Arch* **451**, 116-124, doi:10.1007/s00424-005-1442-2 (2005).

10 Zheng, J. Molecular mechanism of TRP channels. *Compr Physiol* **3**, 221-242, doi:10.1002/cphy.c120001 (2013).

11 Vazquez, G., Wedel, B. J., Aziz, O., Trebak, M. & Putney, J. W., Jr. The mammalian TRPC cation channels. *Biochim Biophys Acta* **1742**, 21-36, doi:10.1016/j.bbamcr.2004.08.015 (2004).

12 Hofmann, T., Schaefer, M., Schultz, G. & Gudermann, T. Subunit composition of mammalian transient receptor potential channels in living cells. *Proc Natl Acad Sci U S A* **99**, 7461-7466, doi:10.1073/pnas.102596199 (2002).

13 Hofmann, T. *et al.* Direct activation of human TRPC6 and TRPC3 channels by

diacylglycerol. *Nature* **397**, 259-263, doi:10.1038/16711 (1999).

14 Eder, P. & Molkentin, J. D. TRPC channels as effectors of cardiac hypertrophy. *Circ Res* **108**, 265-272, doi:10.1161/CIRCRESAHA.110.225888 (2011).

15 Onohara, N. *et al.* TRPC3 and TRPC6 are essential for angiotensin II-induced cardiac hypertrophy. *EMBO J* **25**, 5305-5316, doi:10.1038/sj.emboj.7601417 (2006).

16 Seo, K. *et al.* Combined TRPC3 and TRPC6 blockade by selective small-molecule or genetic deletion inhibits pathological cardiac hypertrophy. *Proc Natl Acad Sci U S A* **111**, 1551-1556, doi:10.1073/pnas.1308963111 (2014).

17 Nakayama, H., Wilkin, B. J., Bodi, I. & Molkentin, J. D. Calcineurin-dependent cardiomyopathy is activated by TRPC in the adult mouse heart. *FASEB J* **20**, 1660-1670, doi:10.1096/fj.05-5560com (2006).

18 Kuwahara, K. *et al.* TRPC6 fulfills a calcineurin signaling circuit during pathologic cardiac remodeling. *J Clin Invest* **116**, 3114-3126, doi:10.1172/JCI27702 (2006).

19 Morine, K. J. *et al.* Endoglin selectively modulates transient receptor potential channel expression in left and right heart failure. *Cardiovasc Pathol* **25**, 478-482, doi:10.1016/j.carpath.2016.08.004 (2016).

20 Kitajima, N. *et al.* TRPC3 positively regulates reactive oxygen species driving maladaptive cardiac remodeling. *Sci Rep* **6**, 37001, doi:10.1038/srep37001 (2016).

21 Sudi, S. B. *et al.* TRPC3-Nox2 axis mediates nutritional deficiency-induced cardiomyocyte atrophy. *Sci Rep* **9**, 9785, doi:10.1038/s41598-019-46252-2 (2019).

22 Oda, S. *et al.* TRPC6 counteracts TRPC3-Nox2 protein complex leading to attenuation of hyperglycemia-induced heart failure in mice. *Sci Rep* **7**, 7511, doi:10.1038/s41598-017-07903-4 (2017).

23 Birnbaumer, L. From GTP and G proteins to TRPC channels: a personal account. *J Mol Med (Berl)* **93**, 941-953, doi:10.1007/s00109-015-1328-5 (2015).

24 Dietrich, A. *et al.* Increased vascular smooth muscle contractility in TRPC6-/- mice. *Mol Cell Biol* **25**, 6980-6989, doi:10.1128/MCB.25.16.6980-6989.2005 (2005).

25 Hartmann, J. *et al.* TRPC3 channels are required for synaptic transmission and motor coordination. *Neuron* **59**, 392-398, doi:10.1016/j.neuron.2008.06.009 (2008).

26 Omatsu-Kanbe, M., Yoshioka, K., Fukunaga, R., Sagawa, H. & Matsuura, H. A simple antegrade perfusion method for isolating viable single cardiomyocytes from neonatal to aged mice. *Physiol Rep* **6**, e13688, doi:10.14814/phy2.13688 (2018).

27 Iribe, G., Kaneko, T., Yamaguchi, Y. & Naruse, K. Load dependency in force-length relations in isolated single cardiomyocytes. *Prog Biophys Mol Biol* **115**, 103-114, doi:10.1016/j.pbiomolbio.2014.06.005 (2014).

28 Yamaguchi, Y. *et al.* TRPC3 participates in angiotensin II type 1 receptor-dependent stress-

induced slow increase in intracellular Ca(2+) concentration in mouse cardiomyocytes. *J Physiol Sci* **68**, 153-164, doi:10.1007/s12576-016-0519-3 (2018).

29 Iribe, G., Kaihara, K., Ito, H. & Naruse, K. Effect of azelnidipine and amlodipine on single cell mechanics in mouse cardiomyocytes. *Eur J Pharmacol* **715**, 142-146, doi:10.1016/j.ejphar.2013.05.030 (2013).

30 Klarenbeek, J., Goedhart, J., van Batenburg, A., Groenewald, D. & Jalink, K. Fourth-generation epac-based FRET sensors for cAMP feature exceptional brightness, photostability and dynamic range: characterization of dedicated sensors for FLIM, for ratiometry and with high affinity. *PLoS One* **10**, e0122513, doi:10.1371/journal.pone.0122513 (2015).

31 Kuroda, T. *et al.* Identification of a Gene Encoding Slow Skeletal Muscle Troponin T as a Novel Marker for Immortalization of Retinal Pigment Epithelial Cells. *Sci Rep* **7**, 8163, doi:10.1038/s41598-017-08014-w (2017).

32 Gibon, J. *et al.* The over-expression of TRPC6 channels in HEK-293 cells favours the intracellular accumulation of zinc. *Biochim Biophys Acta* **1808**, 2807-2818, doi:10.1016/j.bbamem.2011.08.013 (2011).

33 Swaminath, G., Steenhuis, J., Kobilka, B. & Lee, T. W. Allosteric modulation of beta2-adrenergic receptor by Zn(2+). *Mol Pharmacol* **61**, 65-72, doi:10.1124/mol.61.1.65 (2002).

34 Aizenman, E. *et al.* Induction of neuronal apoptosis by thiol oxidation: putative role of intracellular zinc release. *J Neurochem* **75**, 1878-1888, doi:10.1046/j.1471-4159.2000.0751878.x (2000).

35 O'Connell, T. D. *et al.* The alpha(1A/C)- and alpha(1B)-adrenergic receptors are required for physiological cardiac hypertrophy in the double-knockout mouse. *J Clin Invest* **111**, 1783-1791, doi:10.1172/JCI16100 (2003).

36 Inoue, R. *et al.* The transient receptor potential protein homologue TRP6 is the essential component of vascular alpha(1)-adrenoceptor-activated Ca(2+)-permeable cation channel. *Circ Res* **88**, 325-332, doi:10.1161/01.res.88.3.325 (2001).

37 Suzuki, F., Morishima, S., Tanaka, T. & Muramatsu, I. Snapin, a new regulator of receptor signaling, augments alpha1A-adrenoceptor-operated calcium influx through TRPC6. *J Biol Chem* **282**, 29563-29573, doi:10.1074/jbc.M702063200 (2007).

38 Jakob, H., Nawrath, H. & Rupp, J. Adrenoceptor-mediated changes of action potential and force of contraction in human isolated ventricular heart muscle. *Br J Pharmacol* **94**, 584-590, doi:10.1111/j.1476-5381.1988.tb11564.x (1988).

39 Alexander, R. W., Williams, L. T. & Lefkowitz, R. J. Identification of cardiac beta-adrenergic receptors by (minus) [3H]alprenolol binding. *Proc Natl Acad Sci U S A* **72**, 1564-1568, doi:10.1073/pnas.72.4.1564 (1975).

40 Allwood, M. J., Cobbold, A. F. & Ginsburg, J. Peripheral vascular effects of noradrenaline, isopropylnoradrenaline and dopamine. *Br Med Bull* **19**, 132-136, doi:10.1093/oxfordjournals.bmb.a070031 (1963).

41 Mohl, M. C. *et al.* Regulation of murine cardiac contractility by activation of alpha(1A)-adrenergic receptor-operated Ca(2+) entry. *Cardiovasc Res* **91**, 310-319, doi:10.1093/cvr/cvr081 (2011).

42 Lanfranchi, P. A. & Somers, V. K. Arterial baroreflex function and cardiovascular variability: interactions and implications. *Am J Physiol Regul Integr Comp Physiol* **283**, R815-826, doi:10.1152/ajpregu.00051.2002 (2002).

43 Kaufmann, H., Norcliffe-Kaufmann, L. & Palma, J. A. Baroreflex Dysfunction. *N Engl J Med* **382**, 163-178, doi:10.1056/NEJMra1509723 (2020).

44 Lin, M. S., McNay, J. L., Shepherd, A. M., Musgrave, G. E. & Keeton, T. K. Increased plasma norepinephrine accompanies persistent tachycardia after hydralazine. *Hypertension* **5**, 257-263, doi:10.1161/01.hyp.5.2.257 (1983).

45 de Lucia, C., Eguchi, A. & Koch, W. J. New Insights in Cardiac beta-Adrenergic Signaling During Heart Failure and Aging. *Front Pharmacol* **9**, 904, doi:10.3389/fphar.2018.00904 (2018).

46 Lohse, M. J., Engelhardt, S. & Eschenhagen, T. What is the role of beta-adrenergic signaling in heart failure? *Circ Res* **93**, 896-906, doi:10.1161/01.RES.0000102042.83024.CA (2003).

47 Andreini, C., Banci, L., Bertini, I. & Rosato, A. Counting the zinc-proteins encoded in the human genome. *J Proteome Res* **5**, 196-201, doi:10.1021/pr050361j (2006).

48 Hara, T. *et al.* Physiological roles of zinc transporters: molecular and genetic importance in zinc homeostasis. *J Physiol Sci* **67**, 283-301, doi:10.1007/s12576-017-0521-4 (2017).

49 Kambe, T., Tsuji, T., Hashimoto, A. & Itsumura, N. The Physiological, Biochemical, and Molecular Roles of Zinc Transporters in Zinc Homeostasis and Metabolism. *Physiol Rev* **95**, 749-784, doi:10.1152/physrev.00035.2014 (2015).

50 Yamasaki, S. *et al.* Zinc is a novel intracellular second messenger. *J Cell Biol* **177**, 637-645, doi:10.1083/jcb.200702081 (2007).

51 Frederickson, C. J., Koh, J. Y. & Bush, A. I. The neurobiology of zinc in health and disease. *Nat Rev Neurosci* **6**, 449-462, doi:10.1038/nrn1671 (2005).

52 Turan, B. & Tuncay, E. Impact of Labile Zinc on Heart Function: From Physiology to Pathophysiology. *Int J Mol Sci* **18**, doi:10.3390/ijms18112395 (2017).

53 Diallinas, G. Understanding transporter specificity and the discrete appearance of channel-like gating domains in transporters. *Front Pharmacol* **5**, 207, doi:10.3389/fphar.2014.00207 (2014).

54 Inoue, K., O'Bryant, Z. & Xiong, Z. G. Zinc-permeable ion channels: effects on intracellular

zinc dynamics and potential physiological/pathophysiological significance. *Curr Med Chem* **22**, 1248-1257, doi:10.2174/0929867322666150209153750 (2015).

55 Hu, H., Bandell, M., Petrus, M. J., Zhu, M. X. & Patapoutian, A. Zinc activates damage-sensing TRPA1 ion channels. *Nat Chem Biol* **5**, 183-190, doi:10.1038/nchembio.146 (2009).

56 Li, M. *et al.* Molecular determinants of Mg^{2+} and Ca^{2+} permeability and pH sensitivity in TRPM6 and TRPM7. *J Biol Chem* **282**, 25817-25830, doi:10.1074/jbc.M608972200 (2007).

57 Swaminath, G., Lee, T. W. & Kobilka, B. Identification of an allosteric binding site for Zn^{2+} on the beta2 adrenergic receptor. *J Biol Chem* **278**, 352-356, doi:10.1074/jbc.M206424200 (2003).

58 Dunser, M. W. & Hasibeder, W. R. Sympathetic overstimulation during critical illness: adverse effects of adrenergic stress. *J Intensive Care Med* **24**, 293-316, doi:10.1177/0885066609340519 (2009).

59 Akashi, Y. J. *et al.* 123I-MIBG myocardial scintigraphy in patients with "takotsubo" cardiomyopathy. *J Nucl Med* **45**, 1121-1127 (2004).

60 Wittstein, I. S. *et al.* Neurohumoral features of myocardial stunning due to sudden emotional stress. *N Engl J Med* **352**, 539-548, doi:10.1056/NEJMoa043046 (2005).

61 Ghadri, J. R. *et al.* International Expert Consensus Document on Takotsubo Syndrome (Part I): Clinical Characteristics, Diagnostic Criteria, and Pathophysiology. *Eur Heart J* **39**, 2032-2046, doi:10.1093/eurheartj/ehy076 (2018).

62 Watanabe, H. *et al.* Impact of earthquakes on Takotsubo cardiomyopathy. *JAMA* **294**, 305-307, doi:10.1001/jama.294.3.305 (2005).

63 Templin, C. *et al.* Clinical Features and Outcomes of Takotsubo (Stress) Cardiomyopathy. *N Engl J Med* **373**, 929-938, doi:10.1056/NEJMoa1406761 (2015).

64 Pelliccia, F., Kaski, J. C., Crea, F. & Camici, P. G. Pathophysiology of Takotsubo Syndrome. *Circulation* **135**, 2426-2441, doi:10.1161/CIRCULATIONAHA.116.027121 (2017).

65 Luttrell, L. M. & Lefkowitz, R. J. The role of beta-arrestins in the termination and transduction of G-protein-coupled receptor signals. *J Cell Sci* **115**, 455-465 (2002).

66 Kotlikoff, M. I. & Kamm, K. E. Molecular mechanisms of beta-adrenergic relaxation of airway smooth muscle. *Annu Rev Physiol* **58**, 115-141, doi:10.1146/annurev.ph.58.030196.000555 (1996).

67 Cypess, A. M. *et al.* Activation of human brown adipose tissue by a beta3-adrenergic receptor agonist. *Cell Metab* **21**, 33-38, doi:10.1016/j.cmet.2014.12.009 (2015).

68 Lynch, G. S. & Ryall, J. G. Role of beta-adrenoceptor signaling in skeletal muscle: implications for muscle wasting and disease. *Physiol Rev* **88**, 729-767, doi:10.1152/physrev.00028.2007 (2008).

69 Shiuchi, T. *et al.* Induction of glucose uptake in skeletal muscle by central leptin is mediated

by muscle beta2-adrenergic receptor but not by AMPK. *Sci Rep* **7**, 15141, doi:10.1038/s41598-017-15548-6 (2017).

Figures and Figure legends

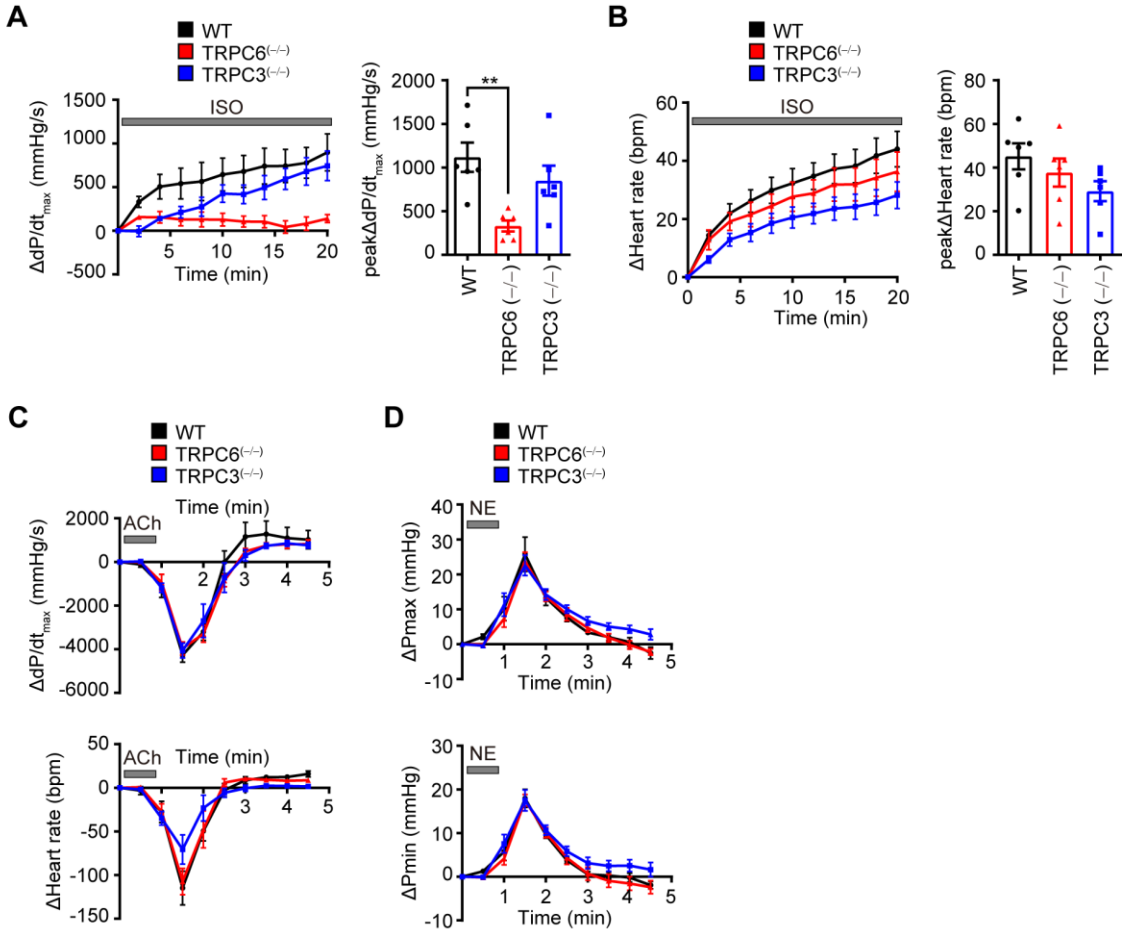

Fig.1 Deletion of TRPC6 reduces positive inotropic effects in mouse hearts

(**A** and **B**) Average time courses of increases in left ventricular contractility (ΔdP/dt max) (**A**, left), peak increases in ΔdP/dtmax (**A**, right) and average time courses of increases in heart rate (Δheart rate) (**B**, left), peak increases in Δheart rate (**B**, right) by βAR stimulation. Mice were injected with isoproterenol (ISO; 10 pg/g/min, 0.05 mL/h) intravenously. (**C**) Average time courses of ΔdP/dt max (top) and Δheart rate (bottom) following *i.v.* administration of acetylcholine (ACh; 0.5 mg/kg, 1.8 mL/h). (**D**) Average time courses of increases in systolic aortic pressure (ΔPmax; top) and diastolic aortic pressure (ΔPmin; bottom) following *i.v.* administration of norepinephrine (NE; 0.05 mg/kg, 1.8 mL/h). WT n=6; TRPC6$^{(-/-)}$ n=6; TRPC3$^{(-/-)}$ n=6. Data are shown as the means ±SEM. **P<0.01 by one-way ANOVA.

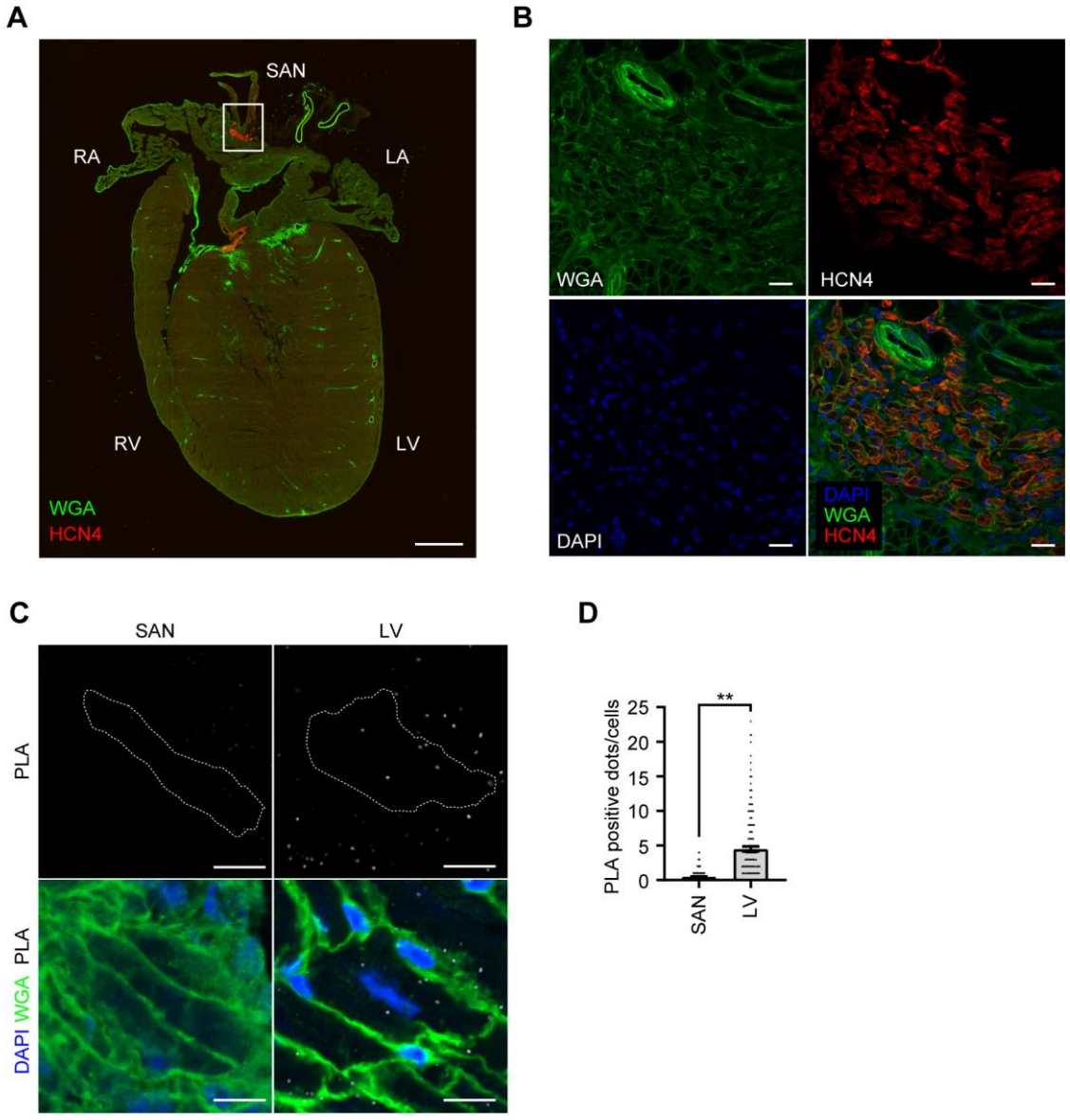
A
SAN
RA
LA
RV
LV
WGA
HCN4
B
WGA
HCN4
DAPI
DAPI
WGA
HCN4
C
SAN
LV
PLA
DAPI WGA PLA
D
PLA positive dots/cells
25
20
15
10
5
0
**
SAN
LV

Fig.2 TRPC6 exists in close proximity to β_1AR in LV myocardium

(**A**) Fluorescence image of whole heart section stained with Alexa Fluor 488-conjugated wheat germ agglutinin (WGA, green) and potassium/sodium hyperpolarization-activated cyclic nucleotide-gated channel 4 (HCN4, red). Boxed area is magnified on (**B**). Scale bar,1 mm. SAN, sinoatrial node; RA, right atrium; RV, right ventricle; LA, left atrium; LV, left ventricle. (**B**) Magnified images of SAN region from (**A**). Green, WGA; red, HCN4; blue, DAPI. Scale bars, 20 μm. (**C**) Representative images of Duolink proximity ligation assay (PLA) between TRPC6 and β_1AR. Cells from SAN (left) and LV (right). PLA signals are shown as white spots, counterstained with WGA (green) and DAPI (blue). In LV group, pictures were captured from apex area. Scale bar, 10 μm. (**D**) The number of PLA signals for each cell from SAN or LV. SAN n=180 cells; LV n=180 cells. Data are shown as the means ±SEM. **P<0.01 by unpaired t test.

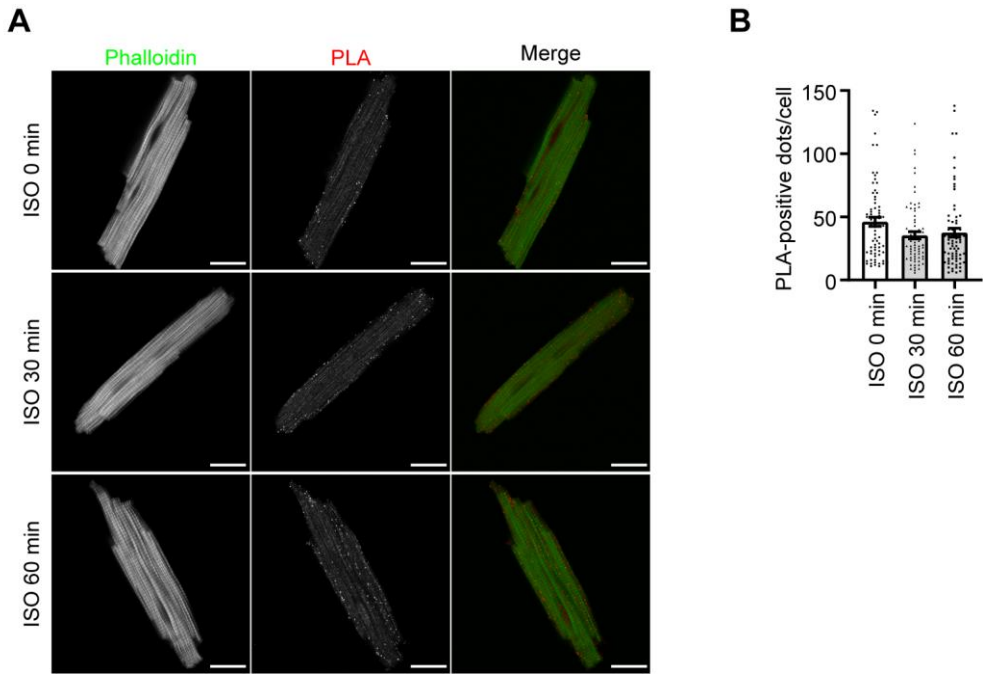

Fig.3 TRPC6 exists in close proximity to β_1AR in isolated mouse cardiomyocytes

(**A**) Representative images of PLA between TRPC6 and β_1AR. PLA signals are colored by red spots (in the merge images), counterstained with phalloidin (green in the merge images). Scale bar, 20 μm. (**B**) The number of PLA-positive signals for each cell before (0 min), 30 or 60 min after ISO (10 nM) treatment. ISO 0 min n=73 cells; 30 min n=72 cells; 60 min n=73 cells.

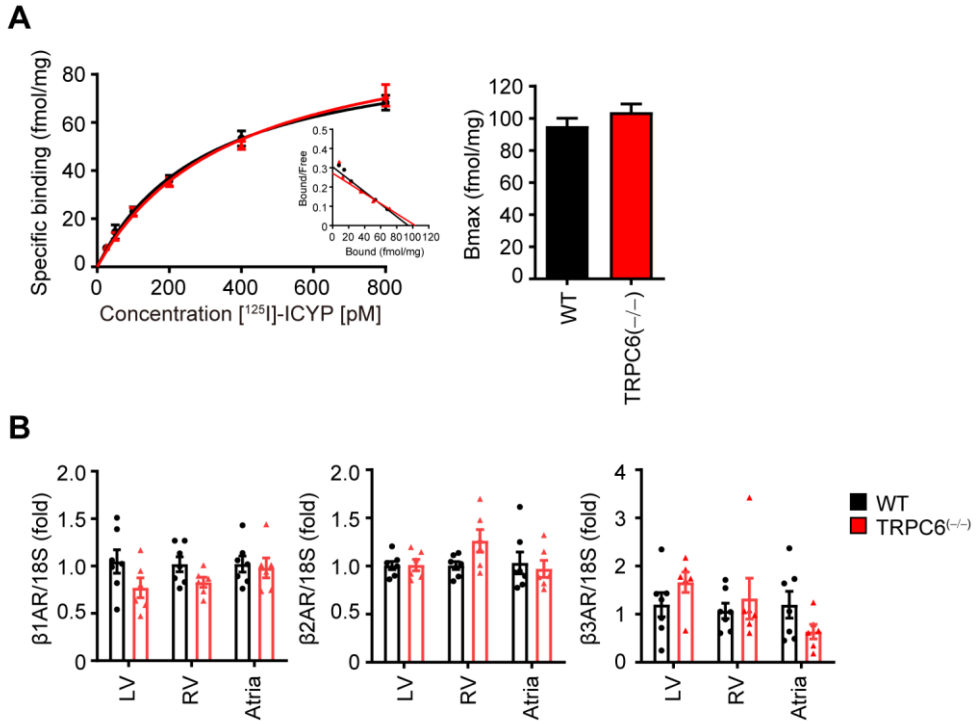

Fig.4 Expression of βAR does not change in TRPC6-deficient mouse hearts

(**A**) Expression levels and binding affinities of βARs in WT and TRPC6$^{(-/-)}$ hearts. WT n=3; TRPC6$^{(-/-)}$ n=3. This result was provided by Dr. A. Nishimura (National Institute for Physiological Sciences).

(**B**) mRNA expression levels of βAR subtypes in LV, RV and atria. mRNA amounts were measured using RT-PCR method. WT n=7; TRPC6$^{(-/-)}$ n=6.

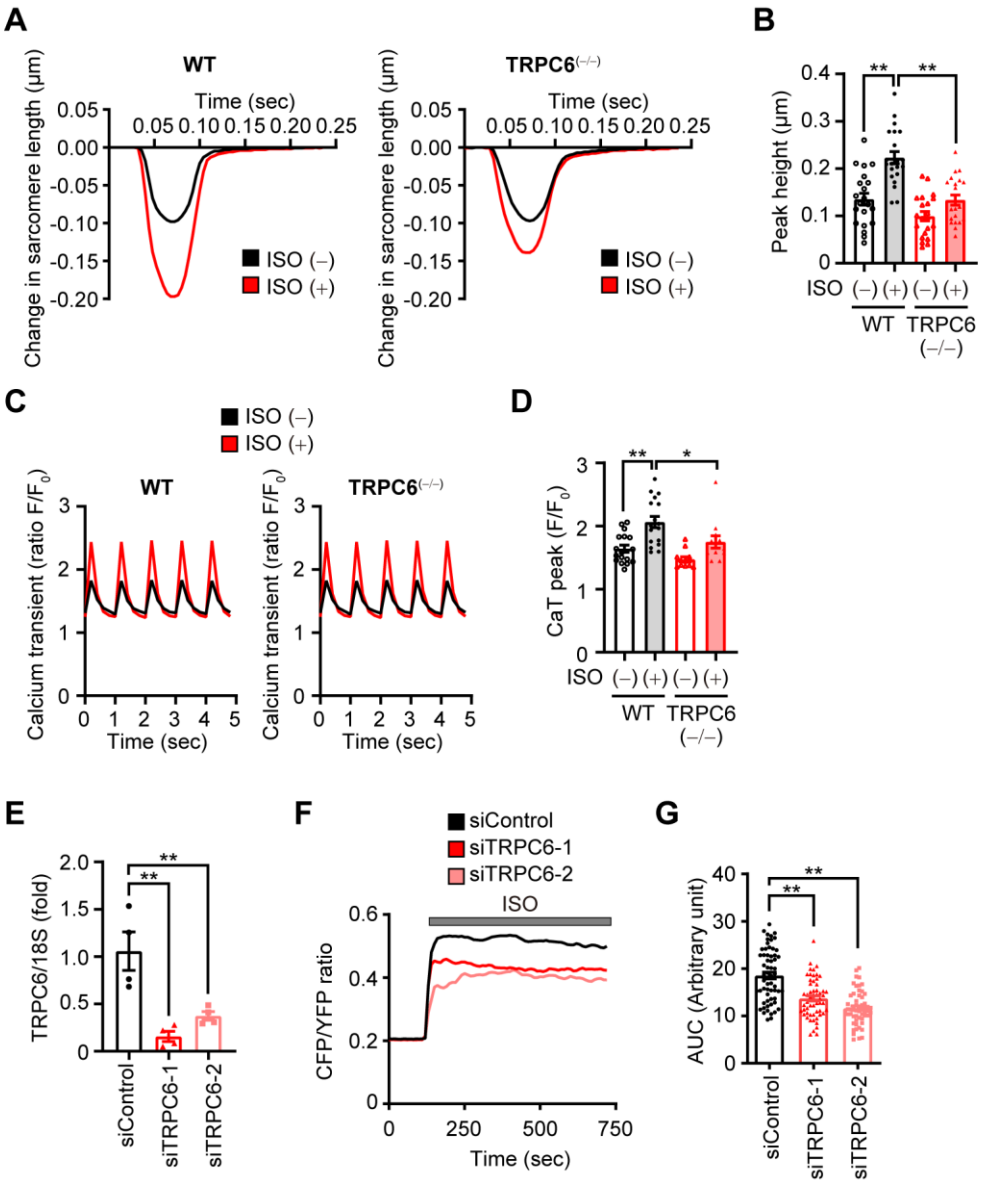
A
WT
TRPC6(–/–)
Time (sec)
0.05 0.10 0.15 0.20 0.25
Change in sarcomere length (μm)
0.05
0.00
-0.05
-0.10
-0.15
-0.20
ISO (–)
ISO (+)
B
Peak height (μm)
0.4
0.3
0.2
0.1
0
**
**
ISO (–) (+) (–) (+)
WT
TRPC6 (–/–)
C
ISO (–)
ISO (+)
WT
TRPC6(–/–)
Calcium transient (ratio F/F0)
3
2
1
0
0 1 2 3 4 5
Time (sec)
D
CaT peak (F/F0)
**
*
ISO (–) (+) (–) (+)
WT TRPC6 (–/–)
E
TRPC6/18S (fold)
2.0
1.5
1.0
0.5
0
**
**
siControl
siTRPC6-1
siTRPC6-2
F
siControl
siTRPC6-1
siTRPC6-2
ISO
CFP/YFP ratio
0.6
0.4
0.2
0
0 250 500 750
Time (sec)
G
AUC (Arbitrary unit)
40
30
20
10
0
**
**
siControl
siTRPC6-1
siTRPC6-2

Fig.5 TRPC6 deletion reduces βAR-stimulated contraction in adult mouse cardiomyocytes.

(**A** and **B**) Representative traces of sarcomere length changes (**A**) and summarized results of peak heights (**B**) induced by ISO (10 nM) stimulation. Isolated mouse cardiomyocytes were excited by field-stimulation at 4 Hz. WT n=21 cells; TRPC6$^{(-/-)}$ n=21 cells. Data were provided by Dr. Y. Yamaguchi and Prof. G. Iribe (Asahikawa Medical University). (**C** and **D**) Representative traces of calcium transient (CaT) (**C**) and summarized results of peak amplitudes of CaT (**D**). Fluo 4 loaded cardiomyocyte were stimulated with ISO (10 nM) under field stimulation at 1 Hz. WT n=17 cells; TRPC6$^{(-/-)}$ n=12 cells. (**E**) mRNA expression level of TRPC6 in siRNA-transfected neonatal rat cardiomyocytes (NRCMs). n=4 each group. (**F** and **G**) Average cAMP production in control or TRPC6-silencing NRCMs (**F**). NRCMs expressing Epac-based FRET biosensor were stimulated with ISO (1 μM). Increases in intracellular cAMP concentrations are shown as area under curve (AUC) (**G**). siControl n=60 cells; siTRPC6#1 n=57 cells; siTRPC6#2 n=55 cells. Epac-based FRET biosensor was gifted by Prof. K. Jalink. Data are shown as the means ±SEM. *P<0.05, **P<0.01 by one-way ANOVA.

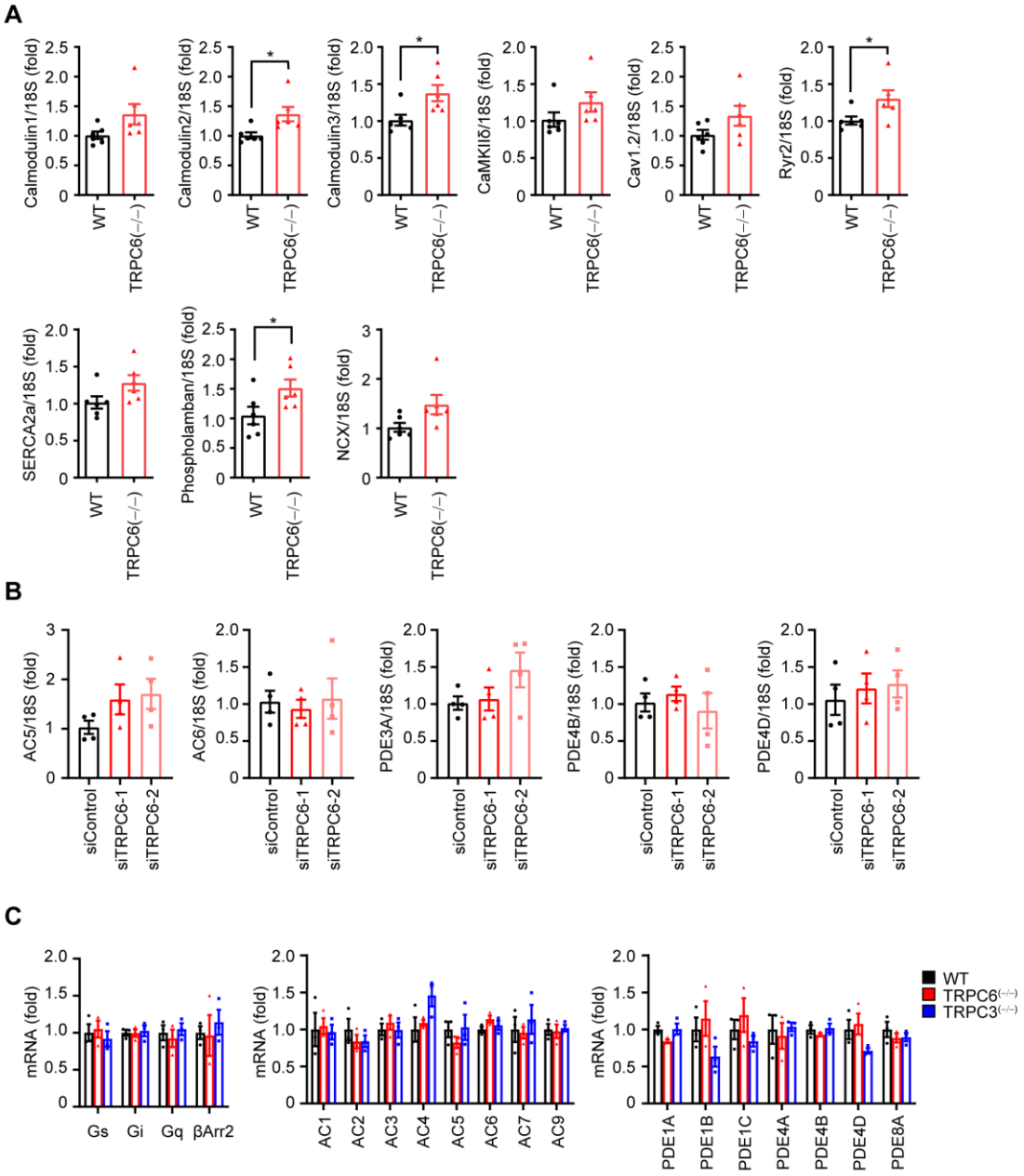
A
Calmodulin1/18S (fold)
Calmodulin2/18S (fold)
Calmodulin3/18S (fold)
CaMKIIδ/18S (fold)
Cav1.2/18S (fold)
Ryr2/18S (fold)
SERCA2a/18S (fold)
Phospholamban/18S (fold)
NCX/18S (fold)
WT
TRPC6(−/−)
B
AC5/18S (fold)
AC6/18S (fold)
PDE3A/18S (fold)
PDE4B/18S (fold)
PDE4D/18S (fold)
siControl
siTRPC6-1
siTRPC6-2
C
mRNA (fold)
Gs
Gi
Gq
βArr2
AC1
AC2
AC3
AC4
AC5
AC6
AC7
AC9
PDE1A
PDE1B
PDE1C
PDE4A
PDE4B
PDE4D
PDE8A
WT
TRPC6(−/−)
TRPC3(−/−)

Fig.6 TRPC6 deletion has little impact on the expression levels of Ca^{2+} handling and Gs-related factors in mouse hearts and NRCMs

(**A**) mRNA expression levels of Ca^{2+} handling-related factors in WT or $TRPC6^{(-/-)}$ mouse hearts. mRNA amounts were measured using RT-PCR method. WT n=6; $TRPC6^{(-/-)}$ n=6. (**B**) mRNA expression levels of adenylate cyclase (AC) and phosphodiesterase (PDE) isoforms in siRNA-treated NRCMs. n=4 each group. (**C**) mRNA expression levels of heterotrimeric G proteins, β-Arrestin 2 (βArr2), and AC and PDE isoforms in adult mouse hearts analyzed by microarray. n=3 each group. This analysis was performed by Dr. Y. Sato and Dr. T. Kuroda (National Institute of Health Sciences). Data are shown as the means ± SEM. *P < 0.05 by unpaired t test.

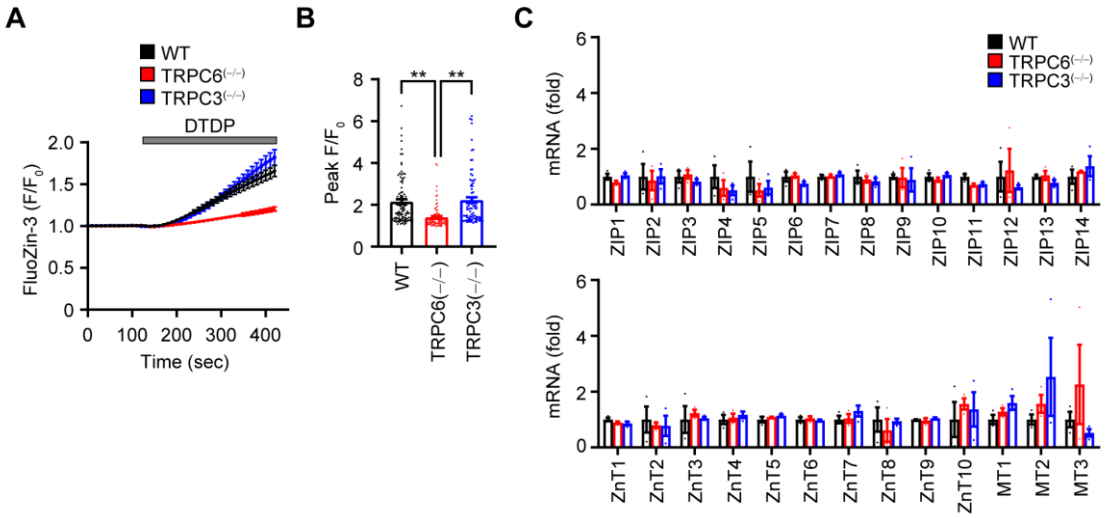

Fig.7 TRPC6-deleted cardiomyocyte contains lower level of intracellular zinc

(**A** and **B**) Average time courses of the FluoZin-3 fluorescence (**A**) and peak increases in fluorescence (**B**) in adult mouse cardiomyocytes. Cardiomyocytes were treated with 2,2′-dithiodipyridine (DTDP, 100 μM). WT n=98 cells; TRPC6$^{(-/-)}$ n=86 cells; TRPC3$^{(-/-)}$ n=84 cells. (**C**) mRNA expression levels of zinc transporters (ZIPs and ZnTs) and metallothioneins (MTs) in mouse hearts analyzed by microarray. n=3 each group. This analysis was performed by Dr. Y. Sato and Dr. T. Kuroda (National Institute of Health Sciences). Data are shown as the means ±SEM. **P<0.01 by one-way ANOVA.

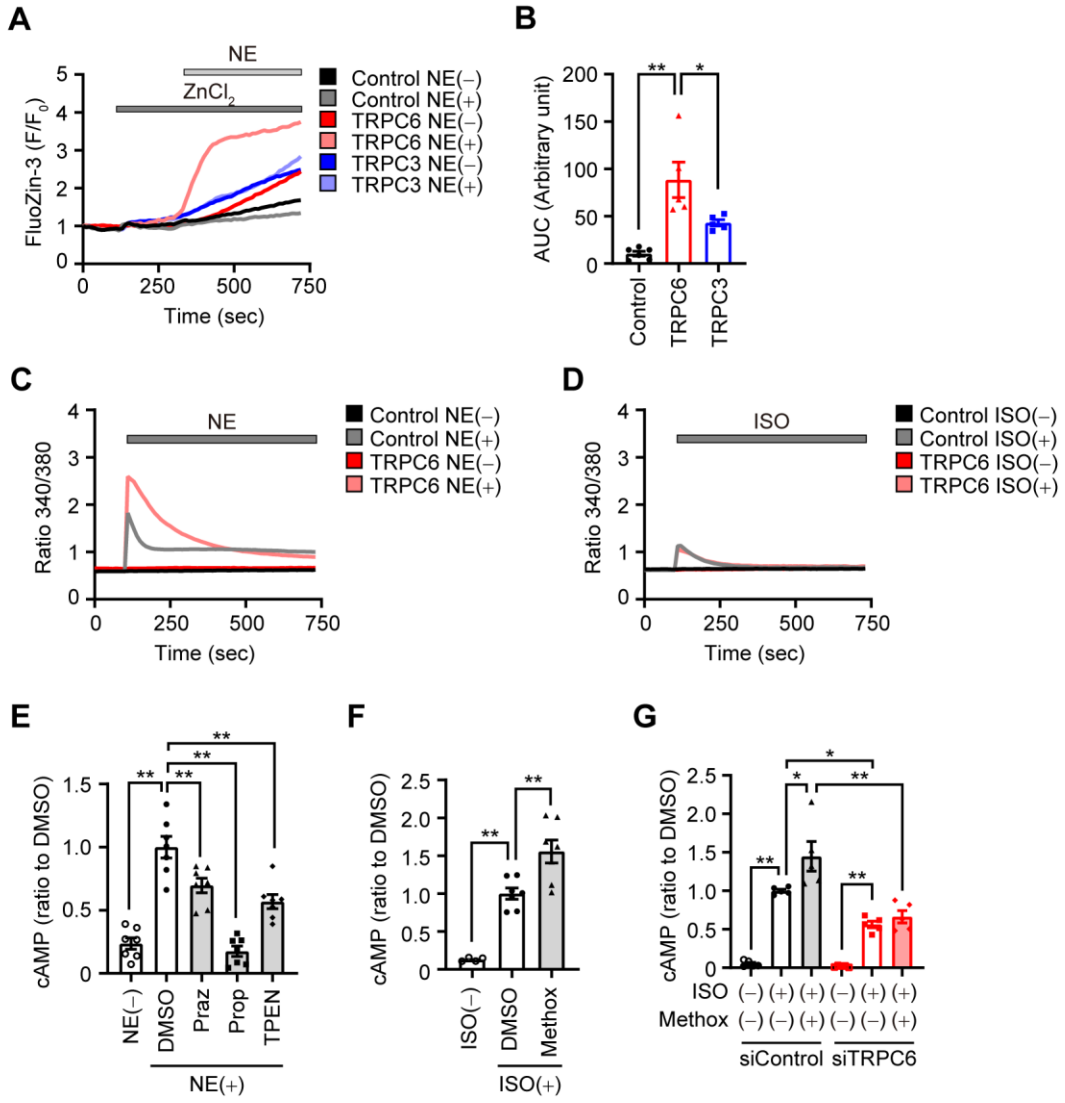
A
NE
ZnCl2
FluoZin-3 (F/F0)
Time (sec)
Control NE(–)
Control NE(+)
TRPC6 NE(–)
TRPC6 NE(+)
TRPC3 NE(–)
TRPC3 NE(+)
B
AUC (Arbitrary unit)
Control
TRPC6
TRPC3
C
NE
Ratio 340/380
Time (sec)
Control NE(–)
Control NE(+)
TRPC6 NE(–)
TRPC6 NE(+)
D
ISO
Ratio 340/380
Time (sec)
Control ISO(–)
Control ISO(+)
TRPC6 ISO(–)
TRPC6 ISO(+)
E
cAMP (ratio to DMSO)
NE(–)
DMSO
Praz
Prop
TPEN
NE(+)
F
cAMP (ratio to DMSO)
ISO(–)
DMSO
Methox
ISO(+)
G
cAMP (ratio to DMSO)
ISO
Methox
siControl
siTRPC6

Fig.8 αAR-TRPC6-Zn^{2+} axis enhances βAR-Gs signaling

(**A** and **B**) Average time courses of changes in intracellular Zn^{2+} concentrations in response to NE stimulation in TRPC-expressing HEK293 cells (**A**). α_{1A} AR and TRPC6/3 co-expressing HEK293 cells were loaded with FluoZin-3 (2 μM) for 30 min at room temperature. $ZnCl_2$ (50 μM) was applied to cells for 3 min before NE stimulation (10 μM). Cumulative increases in FluoZin-3 fluorescence are shown as AUC (**B**). n=5 each group. (**C**) Average traces of intracellular Ca^{2+} concentration in HEK293 cells expressing α_{1A}AR and TRPC6. Cells were stimulated with NE (10 μM). n=3 each group. (**D**) Average traces of intracellular Ca^{2+} concentration in HEK293 cells expressing β_1AR and TRPC6. Cells were stimulated with ISO (10 μM). n=4 each group. (**E**) Changes in intracellular cAMP concentrations by treatment with prazosin (Praz, α_{1A} inhibitor; 10 μM), propranolol (Prop, βAR inhibitor; 10 μM) and TPEN (Zn^{2+} chelator; 25 μM) in NRCMs. NRCMs were treated with prazosin or propranolol for 25 h (including 1-h IBMX treatment, see Material and Method section for the details), or TPEN for 1 h before NE stimulation (1 μM, 30 min). $ZnCl_2$ (50 μM) were included in the culture medium. n=7 each group. (**F**) Intracellular cAMP changes in response to α_1AR stimulation in NRCMs. NRCMs were treated with methoxamine (Methox, 1 μM) for 24 h before ISO stimulation (1 μM, 30 min). $ZnCl_2$ (50 μM) were included in culture medium. n=7 each group (3 samples were below the detection limit in ISO(-) group). (**G**) Requirement of TRPC6 in α_1AR-induced enhancement of βAR-stimulated cAMP production in NRCMs. NRCMs were treated with Methox as mentioned in (**F**). n=5 each group. Data are shown as the means ±SEM. *P<0.05, **P<0.01 by one-way ANOVA.

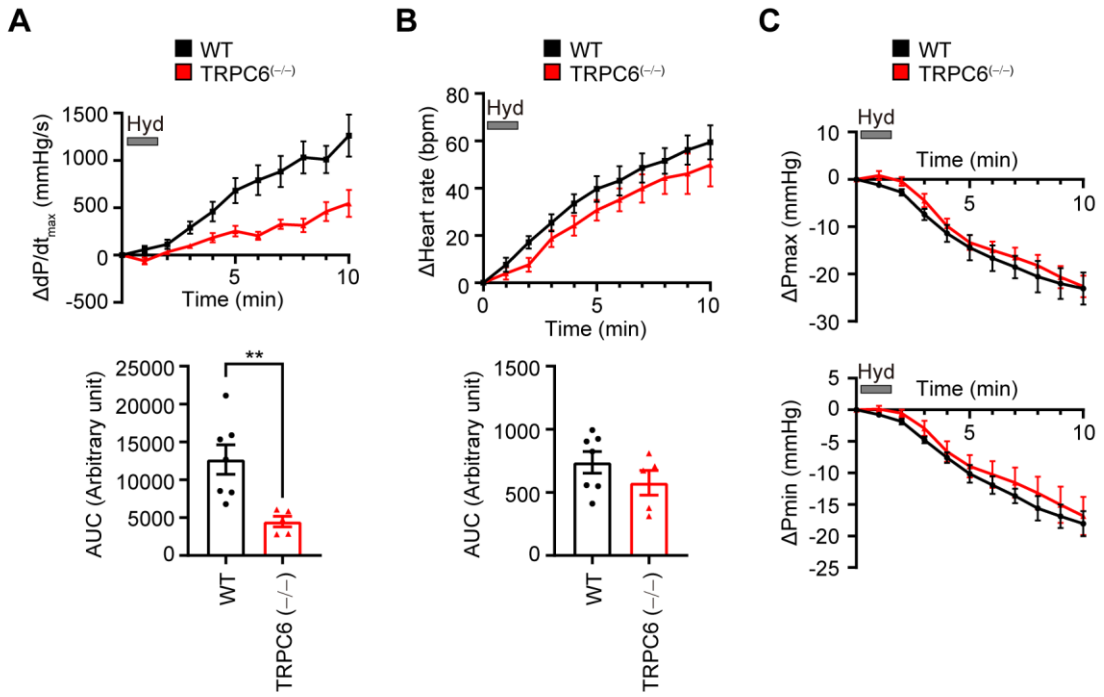

Fig.9 TRPC6 is involved in baroreflex-dependent cardiac contraction.

(**A** and **B**) Average time courses of increases in LV ΔdP/dt max (**A**, top) and Δheart rate (**B**, top) induced by hydralazine administration. Mice were injected with hydralazine (Hyd; 0.5 mg/kg, 1.2 mL/h, *i.v.*). Increases in LV ΔdP/dt max and Δheart rate are shown as AUC (**A**, **B** bottom). WT n=7; TRPC6$^{(-/-)}$ n=5. (**C**) Average time courses of decreases in systolic aortic pressure (ΔPmax; top) and diastolic aortic pressure (ΔPmin; bottom) induced by hydralazine. WT n=5; TRPC6$^{(-/-)}$ n=5. Data are shown as the means ±SEM. **P<0.01 by unpaired t tests.

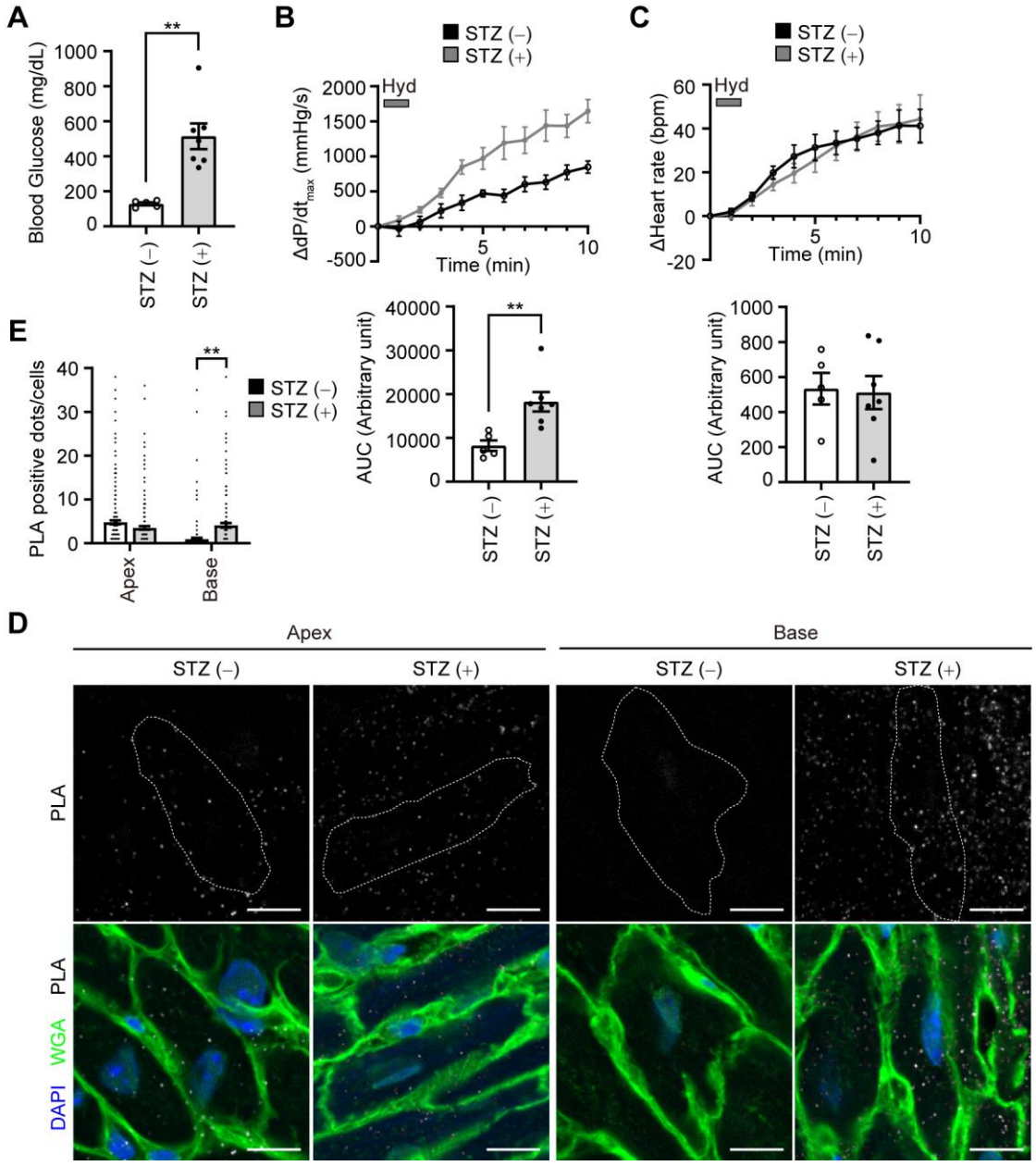
A
Blood Glucose (mg/dL)
1000
800
600
400
200
0
**
STZ (–)
STZ (+)
B
STZ (–)
STZ (+)
Hyd
ΔdP/dtmax (mmHg/s)
2000
1500
1000
500
0
-500
5
10
Time (min)
C
STZ (–)
STZ (+)
Hyd
ΔHeart rate (bpm)
60
40
20
0
-20
5
10
Time (min)
E
PLA positive dots/cells
40
30
20
10
0
**
STZ (–)
STZ (+)
Apex
Base
AUC (Arbitrary unit)
40000
30000
20000
10000
0
**
STZ (–)
STZ (+)
AUC (Arbitrary unit)
1000
800
600
400
200
0
STZ (–)
STZ (+)
D
Apex
Base
STZ (–)
STZ (+)
STZ (–)
STZ (+)
PLA
PLA
WGA
DAPI

Fig.10 TRPC6 upregulation is associated with enhanced baroreflex-dependent cardiac inotropic effect in hyperglycemic mice

(**A**) Blood glucose levels at 4 weeks after streptozotocin (STZ) administration. Mice were injected STZ (50 mg/kg) intraperitoneally for 5 successive days. STZ(-) n=5; STZ(+) n=7. (**B** and **C**) Averaged time course of LV ΔdP/dt max (**B**, top) and averaged time course of Δheart rate (**C**, top) following administration of hydralazine (Hyd; 0.5 mg/kg, 1.2 mL/h, *i.v.*) to mice in a hyperglycemic condition. Increase of LV ΔdP/dt max and Δheart rate are shown as AUC (**B, C** bottom). STZ(-) n=5; STZ(+) n=7. (**D**) Representative images of PLA between TRPC6 and β_1 adrenergic receptor. Cells from apex area (left) and base area (right) in mice with/without STZ. PLA signals are shown as white spots, counterstained with WGA (green) and DAPI (blue). Scale bar, 10 μm. (**E**) The number of PLA signals for each cell from the apex and base area in mice with/without STZ. Apex STZ(-) n=239 cells; Apex STZ(+) n=236 cells; Base STZ(-) n=179 cells; Base STZ(+) n=169 cells. Data are shown as the means ±SEM. **P<0.01 by unpaired t tests.

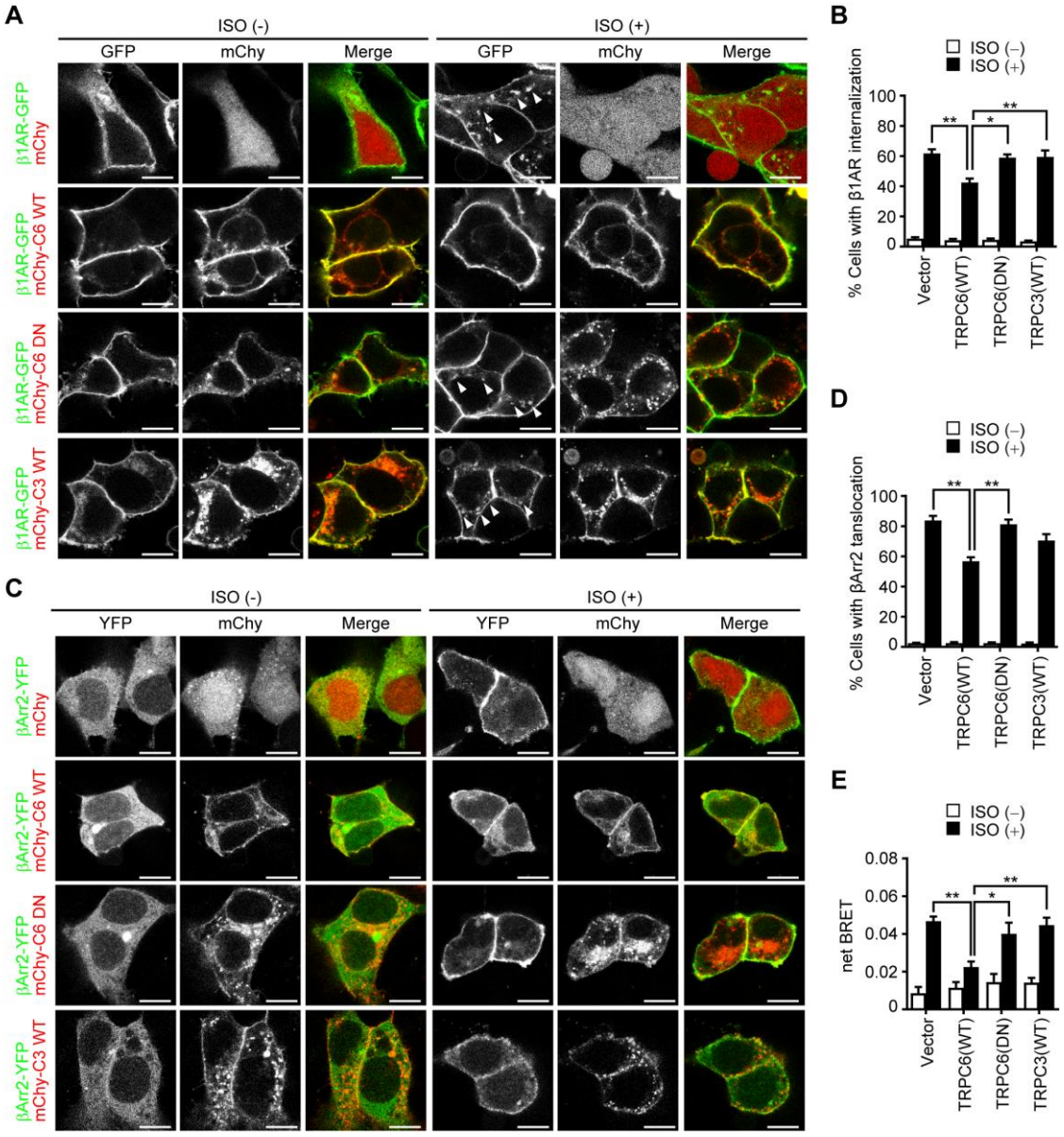
A
ISO (-)
ISO (+)
GFP
mChy
Merge
β1AR-GFP mChy
β1AR-GFP mChy-C6 WT
β1AR-GFP mChy-C6 DN
β1AR-GFP mChy-C3 WT
B
ISO (–)
ISO (+)
% Cells with β1AR internalization
Vector
TRPC6(WT)
TRPC6(DN)
TRPC3(WT)
C
YFP
βArr2-YFP mChy
βArr2-YFP mChy-C6 WT
βArr2-YFP mChy-C6 DN
βArr2-YFP mChy-C3 WT
D
% Cells with βArr2 tanslocation
E
net BRET

Fig.11 TRPC6 suppresses β_1AR internalization after ISO stimulation

(**A** and **B**) Representative images of HEK293 cells co-expressing β_1AR and TRPC6/3 with or without ISO stimulation (**A**). HEK293 were expressed with β_1AR-GFP along with mCherry-tagged TRPC6, pore-dead TRPC6 (dominant negative; DN) or TRPC3. Cells were treated with ISO (10 μM) for 30 min (stimulation condition is same in A to E). Receptor internalization was observed by ISO-dependent redistribution of GFP signals into intracellular space (shown as arrowhead). Quantification of β_1AR-internalizing activity was determined as the ratio of the number of β_1AR-internalized cells to all cells (**B**). n=4 each group. Scale bar, 10 μm. (**C** and **D**) Representative images of HEK293 cells co-expressing βArr2, β_1AR and TRPC6/3 with or without ISO stimulation (**C**). HEK293 cells were expressed with mCherry-tagged TRPC6 or pore-dead TRPC6 or TRPC3 along with YFP-tagged βArr2 (βArr2) and HA-β_1AR. Quantification of βArr2 translocation to plasma membrane was determined as the ratio of the number of cells in which βArr2 were translocated after ISO stimulation to all cells (**D**). n=4 each group. Scale bar, 10 μm. (**E**) Effects of TRPC6/3 on βArr2 recruitment to β_1AR. HEK293 cells were expressed with TRPC6, pore-dead TRPC6 or TRPC3 with β_1AR-Rluc and βArr2-YFP. Cells were stimulated with ISO (10 μM) for 30 min. Vector, TRPC6 (WT), TRPC3 (WT) n=5; TRPC6 (DN) n=4. Data are shown as the means ±SEM. *P<0.05, **P<0.01 by one-way ANOVA.

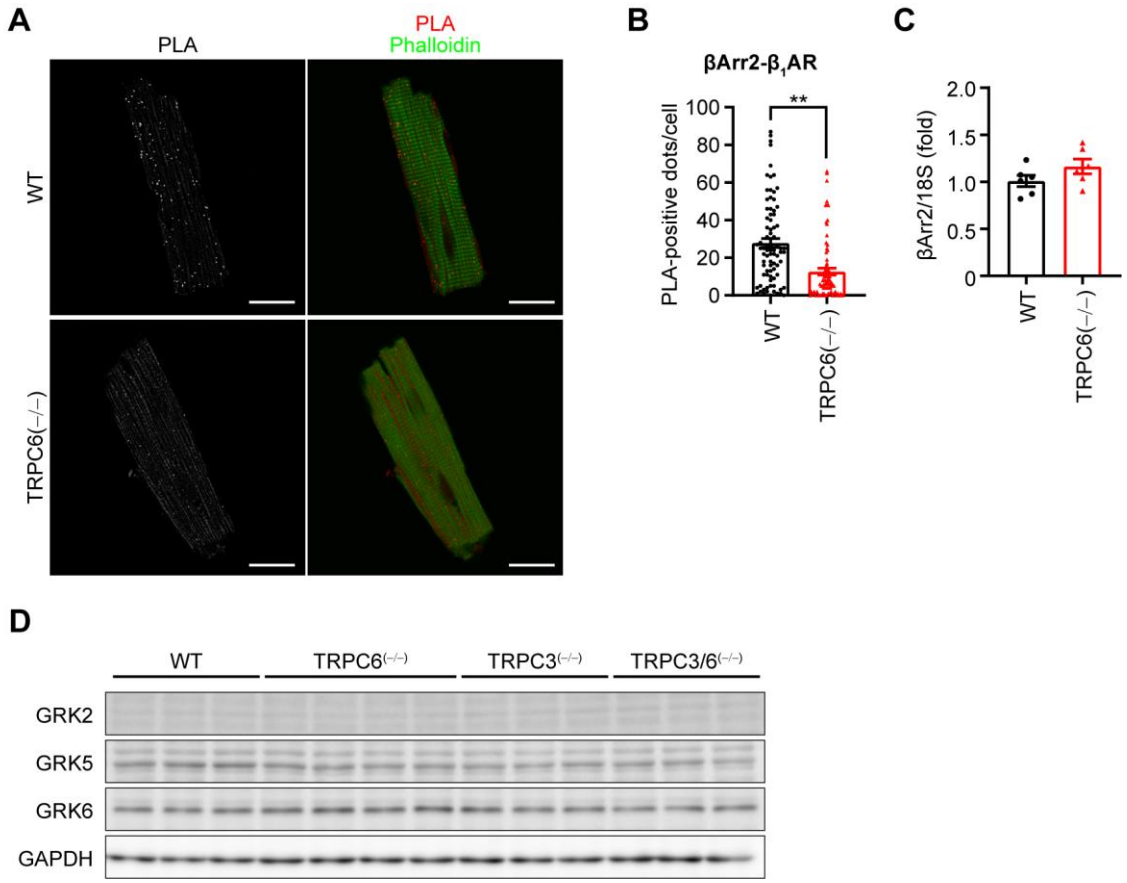

Fig.12 Reduced βArr2-β_1AR interactions in TRPC6-deficient mouse cardiomyocytes

(**A** and **B**) Representative images of PLA between βArr2 and β_1AR in normal WT and TRPC6$^{(-/-)}$ cardiomyocytes. PLA signals were visualized as red spots, counterstained with phalloidin (green) in merged images (**A**). The number of PLA signals for each cell were quantified (**B**). WT n=84 cells; TRPC6$^{(-/-)}$ n=82 cells. Scale bar, 20 μm. (**C**) mRNA expression level of β-arrestin2 in WT and TRPC6$^{(-/-)}$ mouse hearts. mRNA amounts were measured using RT-PCR. WT n=6; TRPC6$^{(-/-)}$ n=6. (**D**) Protein expression levels of G protein-coupled receptor kinase (GRK) subtypes in mouse hearts. WT n=3; TRPC6$^{(-/-)}$ n=4; TRPC3$^{(-/-)}$ n=3; TRPC3/6$^{(-/-)}$ n=3. Data are shown as the means ± SEM. **P < 0.01 by unpaired t test.

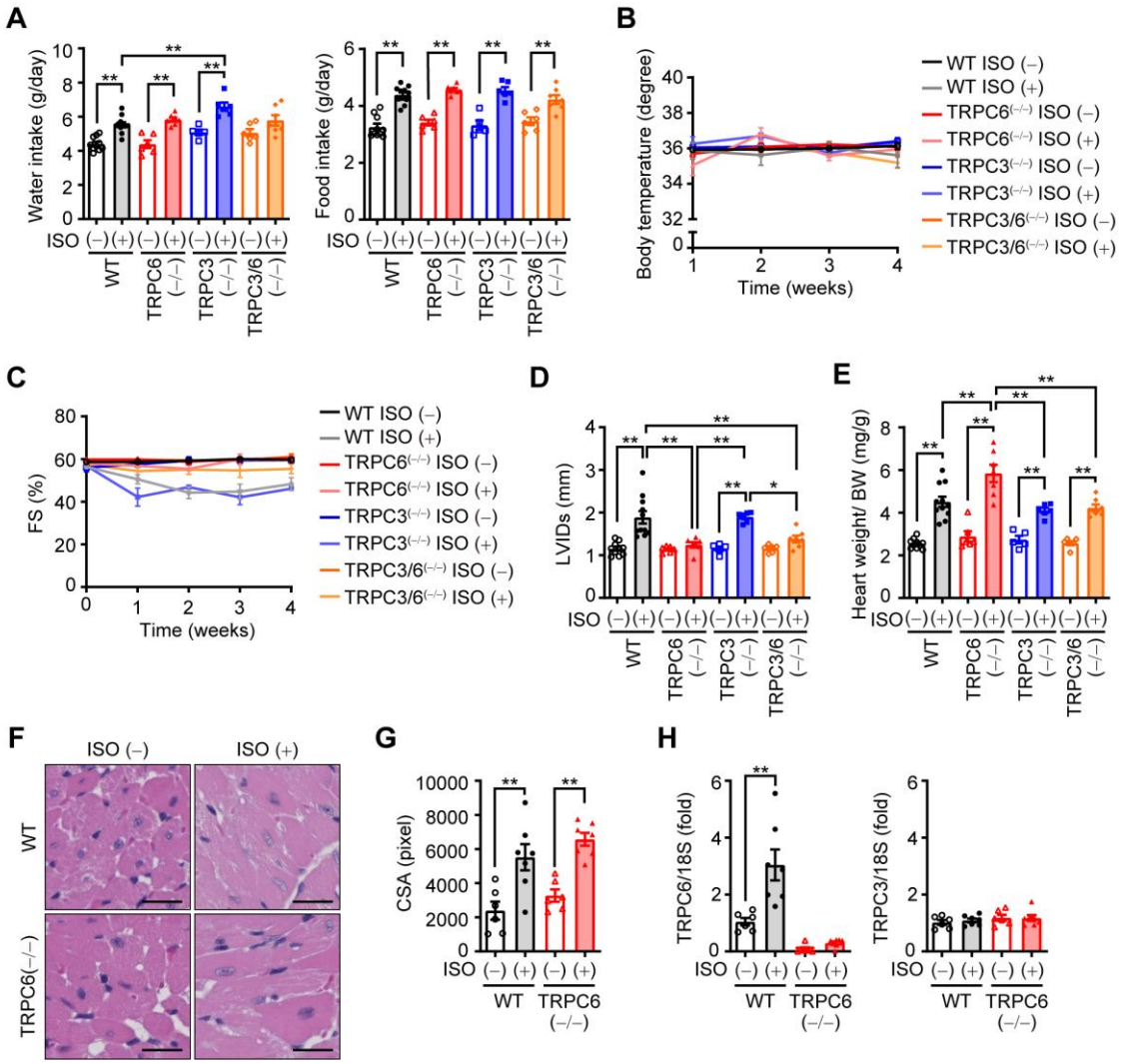
A
Water intake (g/day)
Food intake (g/day)
ISO (–)(+)(–)(+)(–)(+)(–)(+)
WT
TRPC6 (–/–)
TRPC3 (–/–)
TRPC3/6 (–/–)
B
Body temperature (degree)
Time (weeks)
WT ISO (–)
WT ISO (+)
TRPC6(–/–) ISO (–)
TRPC6(–/–) ISO (+)
TRPC3(–/–) ISO (–)
TRPC3(–/–) ISO (+)
TRPC3/6(–/–) ISO (–)
TRPC3/6(–/–) ISO (+)
C
FS (%)
Time (weeks)
D
LVIDs (mm)
E
Heart weight/ BW (mg/g)
F
ISO (–)
ISO (+)
WT
TRPC6(–/–)
G
CSA (pixel)
H
TRPC6/18S (fold)
TRPC3/18S (fold)

Fig.13 TRPC6 participates in cardiac hypertrophy induced by chronic βAR stimulation in mice

(**A**) Daily water and food intake per mouse with or without ISO treatment (30 mg/kg) for 4 weeks. (**B**) Cumulative changes in rectal temperature of mice with or without ISO treatment. (**C** and **D**) Average time courses of changes in LV fractional shortening (FS) (**C**) and LV internal diameter at end-systole (LVIDs) (**D**) 4 weeks after ISO treatment. (**E**) Changes in heart weight / body weight (BW) ratios. WT ISO (-) n=10; WT ISO (+) n=11; TRPC6$^{(-/-)}$ ISO(-) n=6; TRPC6$^{(-/-)}$ ISO(+) n=7; TRPC3$^{(-/-)}$ ISO(-) n=5; TRPC3$^{(-/-)}$ ISO(+) n=6; TRPC3/6$^{(-/-)}$ ISO(-) n=6; TRPC3/6$^{(-/-)}$ ISO(+) n=7 (**A**-**E**). (**F** and **G**) Representative images of heart sections stained with hematoxylin and eosin (H&E) (**F**). Results of cardiomyocyte cross-sectional area (CSA) are shown in (**G**). Scale bar, 20 μm. (**H**) mRNA expression levels of TRPC6 (left) and TRPC3 (right) in mouse hearts. WT ISO (-) n=6; WT ISO (+) n=7; TRPC6$^{(-/-)}$ ISO(-) n=6; TRPC6$^{(-/-)}$ ISO(+) n=7 (**G**, **H**). Data are shown as the means ±SEM. *P<0.05, **P<0.01 by one-way ANOVA.

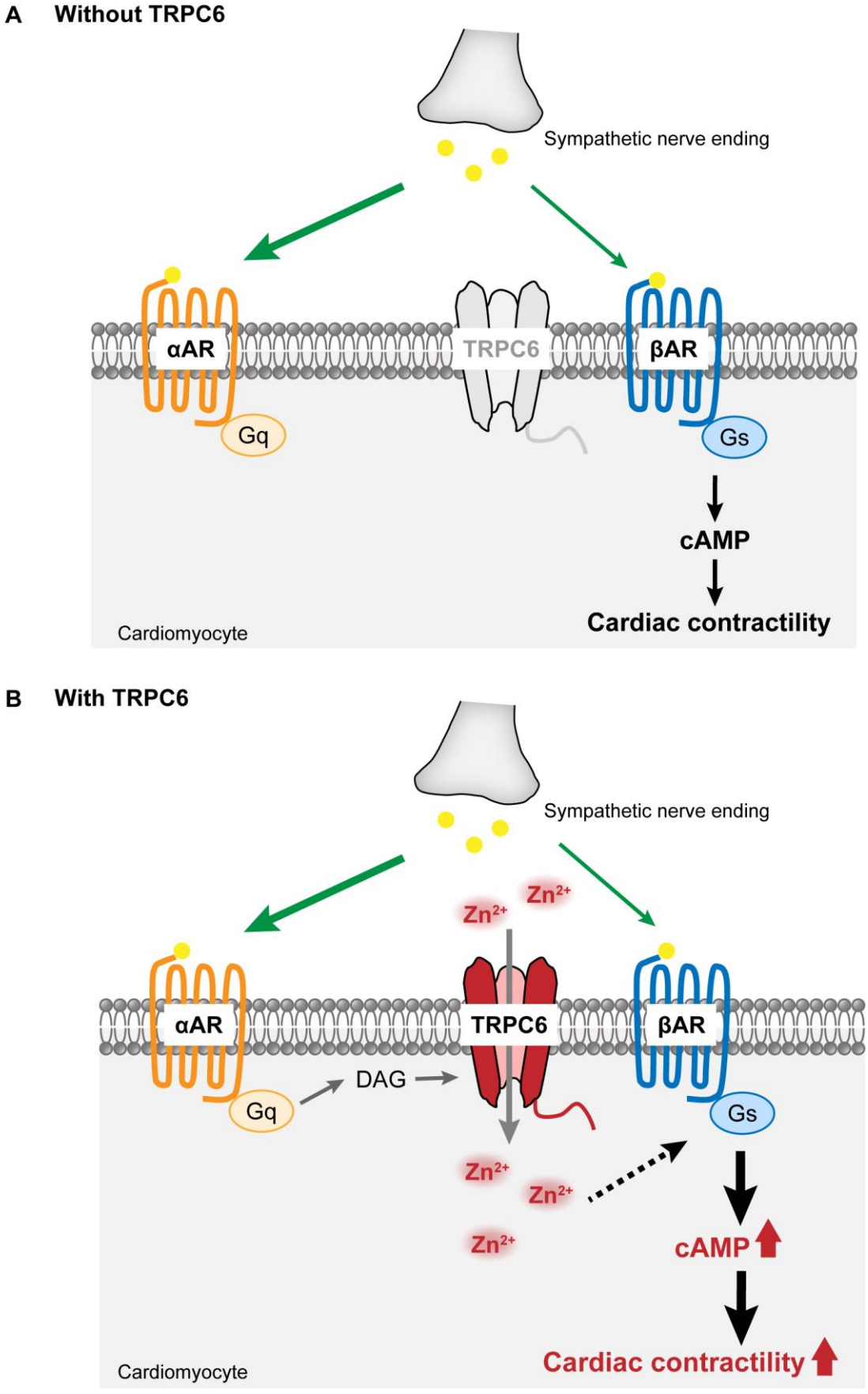
A Without TRPC6
Sympathetic nerve ending
αAR
TRPC6
βAR
Gq
Gs
cAMP
Cardiac contractility
Cardiomyocyte
B With TRPC6
Sympathetic nerve ending
Zn2+
Zn2+
αAR
TRPC6
βAR
DAG
Gq
Gs
Zn2+
Zn2+
Zn2+
cAMP
Cardiac contractility
Cardiomyocyte

Fig.14 Schema of the role of TRPC6-mediated Zn^{2+} influx in adrenergic receptor-stimulated cardiac inotropy

Cardiac inotropy through sympathetic nervous system has been considered to be predominantly mediated by βAR activation, although the chemical binding affinity of NE to βAR is much lower than that to αAR (**A**). This study first demonstrates that αAR-mediated Zn^{2+} influx via TRPC6 promotes NE-induced cardiac inotropy by local Zn^{2+}-dependent enhancement of βAR-Gs signaling (**B**). Down-regulation of αAR-TRPC6-Zn^{2+} axis may result in the reduction of sympathetic nerve-mediated cardiac inotropy (**A**).

Tables

	Antigen	**Host**	**Supplier**	**Catalog no.**	**Dilution**	**Usage**
1st	HCN4	Rabbit	Alomone	APC-052	1:100	IF
	TRPC6	Mouse	Santa Cruz	sc-515837	1:50	PLA
	β_1AR	Rabbit	Abcam	ab3442	1:150	PLA
	βArr2	Mouse	Santa Cruz	sc-365445	1:50	PLA
	GRK2	Rabbit	Cell Signaling Technology	3982S	1:2000	WB
	GRK5	Rabbit	Bosterbio	PB9708	1:2000	WB
	GRK6	Rabbit	Cell Signaling Technology	5878S	1:2000	WB
	GAPDH	Rabbit	Cell Signaling Technology	2118S	1:3000	WB
2nd	anti-Rabbit IgG, Alexa Fluor 594		Invitrogen™	A-11037	1:200	IF
	anti-Rabbit IgG, HRP-linked Antibody		Cell Signaling Technology	7074	1:8000	WB

Table.1 List of antibody for immunostaining and Western Blot

IF, Immunofluorescence; PLA, Proximity ligation assay; WB, Western blotting

Primers for SYBR green	**Sequence**	
Mouse β_1AR	Forward	ATCTCTGTTTACTCAAGACCGAAAGCA
	Reverse	CATACTAAGCCACACTCTCCCAACTC
Mouse β_2AR	Forward	AAGTTTACATCCTCCTTAACTGGTTGG
	Reverse	TAGAGTAGCCGTTCCCATAGGTTTT
Mouse β_3AR	Forward	GTTGTCCTGGTGTGGATCGTGT
	Reverse	ATAGGGCATGTTGGAGGCAAAG
Mouse Calmodulin1	Forward	TGGGAATGGTTACATCAGTGC
	Reverse	CGCCATCAATATCTGCTTCTCT
Mouse Calmodulin2	Forward	ACGGGGATGGGACAATAACAA
	Reverse	TGCTGCACTAATATAGCCATTGC
Mouse Calmodulin3	Forward	GATGGCACCATTACCACCAAG
	Reverse	CGCTGTCTGTATCCTTCATCTTT
Mouse CaMKIIδ	Forward	GCTAGGGACCATCAGAAACTG
	Reverse	GTCTTCAAACAGTTCGCCAC
Mouse Cav1.2	Forward	CCTGCTGGTGGTTAGCGTG
	Reverse	TCTGCCTCCGTCTGTTTAGAA
Mouse Ryanodine receptor 2 (Ryr2)	Forward	ACATCATGTTTTACCGCCTGAG
	Reverse	TTTGTGGTTATTGAACTCTGGCT
Mouse SERCA2a	Forward	GGGCAAAGTGTATCGACAGG
	Reverse	TCAGCAGGAACTTTGTCACC
Mouse Phospholamban	Forward	ATGACGACGATTCAAATCTCTTGG
	Reverse	TGGGTTTGCAAAGTTAGGCATAA
Mouse NCX1	Forward	GGTGAACTGCCTCCAGAGAG
	Reverse	GTGCCAGACACCGTATCCTT
Mouse βArr2	Forward	AAGTCGAGCCCTAACTGCAA
	Reverse	GGTGAGGGTCACGAACACTT
Mouse TRPC6	Forward	GACCGTTCATGAAGTTTGTAGCAC
	Reverse	AGTATTCTTTGGGGCCTTGAGTCC
Mouse TRPC3	Forward	AGCCGAGCCCCTGGAAAGACAC
	Reverse	CCGATGGCGAGGAATGGAAGAC

Primers for SYBR green	Sequence	
Rat Adenylyl cyclase 5 (AC5)	Forward	ACCATTGTGCCCCACTCCCTGTT
	Reverse	TCGTCGCCCAGGCTGTAGTTGAA
Rat Adenylyl cyclase 6 (AC6)	Forward	CTGCTTGTGTTCATCTCTG
	Reverse	GACGCTAAGCAGTAGATCA
Rat Phosphodiesterase 3A (PDE3A)	Forward	TCACAGGGCCTTAACTTACAC
	Reverse	GGAGCAAGAATTGGTTTGTCC
Rat Phosphodiesterase 4B (PDE4B)	Forward	CAGCTCATGACCCAGATAAGTGG
	Reverse	GTCTGCACAATGTACCATGTTGCG
Rat Phosphodiesterase 4D (PDE4D)	Forward	CCTCTGACTGTTATCATGCACACC
	Reverse	GATCCACATCATGTATTGCACTGGC
Rat TRPC6	Forward	TCACTTGGAAGAACAGTGAAAGA
	Reverse	CATCCTCAATTTCCTGGAATGAAC

Table.2. List of primer pairs for RT-PCR

Genotype	Treatment	n	BUN (mg/dL)	ALT (U/L)	AST (U/L)	CPK (U/L)
WT	vehicle	9	30.9 ± 2.2	24.3 ± 1.2	44.6 ± 4.2	249.1 ± 30.6
	ISO	11	24.3 ± 2.0	29.7 ± 1.6[a]	48.5 ± 2.8	224.0 ± 29.5
TRPC6$^{(-/-)}$	vehicle	6	30.1 ± 1.8	21.2 ± 0.7	36.7 ± 1.5	315.7 ± 78.7
	ISO	6	25.6 ± 3.0	24.8 ± 1.1	46.5 ± 2.5	215.0 ± 35.4
TRPC3$^{(-/-)}$	vehicle	5	29.5 ± 1.7	21.6 ± 1.9	38.0 ± 1.3	227.0 ± 28.0
	ISO	6	25.9 ± 2.4	23.0 ± 1.4[c]	43.3 ± 3.0	208.0 ± 14.1
TRPC3/6$^{(-/-)}$	vehicle	6	29.9 ± 2.5	19.5 ± 0.7	37.2 ± 2.4	239.2 ± 24.0
	ISO	7	25.2 ± 1.9	25.7 ± 1.3	52.0 ± 3.0[g]	324.6 ± 42.4

Genotype	Treatment	n	TG (mg/dL)	GLU (mg/dL)	TCHO (mg/dL)
WT	vehicle	9	104.0 ± 15.4	188.7 ± 8.3	77.4 ± 1.7
	ISO	10	27.1 ± 3.8[b]	128.4 ± 15.7	100.4 ± 2.0[b]
TRPC6$^{(-/-)}$	vehicle	6	99.7 ± 18.2	199.3 ± 8.9	80.3 ± 2.6
	ISO	6	36.8 ± 12.1	122.3 ± 21.4	107.3 ± 4.9[d]
TRPC3$^{(-/-)}$	vehicle	5	94.2 ± 15.8	160.4 ± 30.4	76.6 ± 2.9
	ISO	6	16.3 ± 4.1[e]	80.3 ± 20.0	102.2 ± 1.8[f]
TRPC3/6$^{(-/-)}$	vehicle	6	119.3 ± 33.0	181.3 ± 9.8	79.5 ± 3.3
	ISO	7(6)*	16.4 ± 2.2[h]	70.0 ± 20.8[h]	108.8 ± 3.5[h]

* TG n=7; GLU, TCHO n=6

Table 3. Results of plasma parameters of mice treated with ISO for 4 weeks.

BUN, Blood urea nitrogen; ALT, Alanine aminotransferase; AST, Aspartate aminotransferase; CPK, Creatine phosphokinase; TG, Triglyceride; GLU, Glucose; TCHO, Total cholesterol. Data are shown as mean ± SEM. Significance was determined by one-way ANOVA followed by Tukey's comparison test. [a] $P<0.05$ compared with WT vehicle group, [b] $P<0.01$ compared with WT vehicle group, [c] $P<0.05$ compared with WT ISO group, [d] $P<0.01$ compared with TRPC6$^{(-/-)}$ vehicle group, [e] $P<0.05$ compared with TRPC3$^{(-/-)}$ vehicle group, [f] $P<0.01$ compared with TRPC3$^{(-/-)}$ vehicle group, [g] $P<0.05$ compared with TRPC3/6$^{(-/-)}$ vehicle group, [h] $P<0.01$ compared with TRPC3/6$^{(-/-)}$ vehicle group.

Genotype	Treatment	n	HR (bpm)	IVSTd (mm)	LVIDd (mm)	LVIDs (mm)
WT	vehicle	10	617.9 ± 13.2	1.23 ± 0.03	2.85 ± 0.07	1.15 ± 0.05
	ISO	11	595.6 ± 34.6	1.16 ± 0.05	3.62 ± 0.09[b]	1.89 ± 0.15[b]
TRPC6$^{(-/-)}$	vehicle	6	627.5 ± 22.0	1.30 ± 0.04	2.86 ± 0.06	1.14 ± 0.03
	ISO	7	652.9 ± 18.9	1.34 ± 0.05	3.05 ± 0.09[dg]	1.24 ± 0.06[dg]
TRPC3$^{(-/-)}$	vehicle	5	631.7 ± 15.8	1.27 ± 0.06	2.84 ± 0.09	1.15 ± 0.05
	ISO	6	563.9 ± 10.9	1.23 ± 0.08	3.52 ± 0.08[e]	1.90 ± 0.05[e]
TRPC3/6$^{(-/-)}$	vehicle	6	594.5 ± 10.2	1.15 ± 0.03	2.97 ± 0.05	1.15 ± 0.04
	ISO	7	618.1 ± 19.8	1.16 ± 0.04	3.09 ± 0.05[df]	1.38 ± 0.08[df]

Genotype	Treatment	n	LVPWd (mm)	FS (%)	EF (%)
WT	vehicle	10	0.80 ± 0.03	59.6 ± 0.9	92.8 ± 0.5
	ISO	11	0.64 ± 0.05[a]	48.2 ± 3.1[b]	83.5 ± 3.3[b]
TRPC6$^{(-/-)}$	vehicle	6	0.85 ± 0.01	60.2 ± 0.7	93.2 ± 0.3
	ISO	7	1.10 ± 0.07[dgh]	59.4 ± 1.0[dg]	92.7 ± 0.5[cf]
TRPC3$^{(-/-)}$	vehicle	5	0.79 ± 0.05	59.4 ± 0.7	92.8 ± 0.4
	ISO	6	0.66 ± 0.02	46.1 ± 0.8[e]	83.2 ± 0.7
TRPC3/6$^{(-/-)}$	vehicle	6	0.70 ± 0.03	61.1 ± 1.3	93.5 ± 0.6
	ISO	7	0.83 ± 0.04[c]	55.4 ± 2.2	90.0 ± 1.5

Table 4. Echocardiographic parameters of mice treated with ISO for 4 weeks.

HR, Heart rate; IVSTd, Interventricular septum diastolic thickness; LVIDd, Left ventricular internal diameter at end-diastole; LVIDs, Left ventricular internal diameter at end-systole; LVPWd, Left ventricular posterior wall diastolic thickness; FS, Fractional shortening; EF, Ejection fraction. The results of FS and LVIDs were same as shown Fig.13C and D respectively. Data are shown as mean ± SEM. Significance was determined by one-way ANOVA followed by Tukey's comparison test. [a] $P<0.05$ compared with WT vehicle group, [b] $P<0.01$ compared with WT vehicle group, [c] $P<0.05$ compared with WT ISO group, [d] $P<0.01$ compared with WT ISO group, [e] $P<0.01$ compared with TRPC3$^{(-/-)}$ vehicle group, [f] $P<0.05$ compared with TRPC3$^{(-/-)}$ ISO group, [g] $P<0.01$ compared with TRPC3$^{(-/-)}$ ISO group, [h] $P<0.01$ compared with TRPC3/6$^{(-/-)}$ ISO group.

Genotype	Treatment	n	Pmax (mmHg)	Pmin (mmHg)	Pmean (mmHg)	HR (bpm)
WT	vehicle	8	107.9 ± 1.75	4.89 ± 1.38	48.2 ± 2.48	465.4 ± 19.0
	ISO	10	109.4 ± 3.19	8.54 ± 2.09	56.5 ± 3.37	551.5 ± 26.4
TRPC6$^{(-/-)}$	vehicle	6	123.7 ± 3.56	4.76 ± 0.71	58.0 ± 2.36	457.4 ± 7.1
	ISO	6	130.4 ± 3.50^{a,b,c}	8.33 ± 0.81	67.4 ± 2.28	568.2 ± 19.8
TRPC3$^{(-/-)}$	vehicle	5	115.9 ± 3.08	10.10 ± 2.24	57.5 ± 3.55	439.2 ± 24.9
	ISO	5	103.0 ± 3.96	7.66 ± 1.24	52.2 ± 2.57	537.9 ± 38.4
TRPC3/6$^{(-/-)}$	vehicle	6	105.4 ± 5.23	5.85 ± 0.41	49.1 ± 3.44	482.7 ± 15.6
	ISO	6	106.4 ± 6.95	6.60 ± 2.82	50.8 ± 4.71	581.8 ± 22.1

Genotype	Treatment	n	dP/dt max (mmHg/s)	dP/dt min (mmHg/s)	Tau (ms)
WT	vehicle	8	6646 ± 326	-7592 ± 600	9.03 ± 0.66
	ISO	10(9)*	7804 ± 584	-5844 ± 513	11.26 ± 1.66
TRPC6$^{(-/-)}$	vehicle	6	6690 ± 209	-7147 ± 245	9.44 ± 0.34
	ISO	6	8793 ± 475	-6886 ± 704	10.49 ± 0.83
TRPC3$^{(-/-)}$	vehicle	5	5998 ± 363	-6005 ± 604	11.85 ± 1.34
	ISO	5	6745 ± 529	-5225 ± 606	11.75 ± 0.30
TRPC3/6$^{(-/-)}$	vehicle	6	6728 ± 696	-7421 ± 918	8.53 ± 0.71
	ISO	6	8173 ± 595	-6749 ± 643	9.09 ± 1.37

* dP/dt max, dP/dt min n=10; Tau n=9

Table 5. Catheter parameters of mice treated with ISO for 4 weeks.

Pmax, Max pressure; Pmin, Minimum pressure; Pmean, Mean pressure; dP/dt max, Maximal rate of pressure development; dP/dt min, Maximal rate of decay of pressure; tau, Monoexponential time constant of relaxation. Data are shown as mean ± SEM. Significance was determined by one-way ANOVA followed by Tukey's comparison test. [a] $P<0.01$ compared with WT ISO group, [b] $P<0.01$ compared with TRPC3$^{(-/-)}$ vehicle group, [c] $P<0.05$ compared with TRPC3/6$^{(-/-)}$ ISO group.

Genotype	Treatment	n	BW (g)	Organ weight per BW (mg/g)		
				Heart	Lung	Liver
WT	vehicle	10	25.6 ± 0.43	4.27 ± 0.04	5.21 ± 0.10	42.1 ± 1.38
	ISO	11	28.5 ± 0.45[b]	5.25 ± 0.12[b]	5.44 ± 0.09	39.1 ± 0.88
TRPC6$^{(-/-)}$	vehicle	6	26.1 ± 0.83	4.45 ± 0.12	5.18 ± 0.16	42.3 ± 0.65
	ISO	7	28.2 ± 0.63	5.92 ± 0.20[dfko]	5.56 ± 0.34	39.5 ± 1.05
TRPC3$^{(-/-)}$	vehicle	5	25.2 ± 0.82	4.37 ± 0.09	5.26 ± 0.06	40.1 ± 2.75
	ISO	6	28.6 ± 0.57[i]	5.05 ± 0.06[i]	5.19 ± 0.12	35.7 ± 0.77
TRPC3/6$^{(-/-)}$	vehicle	6	26.8 ± 0.39	4.28 ± 0.05	4.96 ± 0.08	43.0 ± 0.87
	ISO	7	28.1 ± 0.50	5.11 ± 0.08[m]	5.44 ± 0.23	36.3 ± 0.86[l]

Genotype	Treatment	n	Organ weight per BW (mg/g)		
			Kidney	Spleen	BAT
WT	vehicle	10	6.73 ± 0.13	2.39 ± 0.08	3.04 ± 0.15
	ISO	11	6.28 ± 0.13	2.31 ± 0.05	3.53 ± 0.13
TRPC6$^{(-/-)}$	vehicle	6	6.34 ± 0.13	2.03 ± 0.06	2.90 ± 0.19
	ISO	7	5.89 ± 0.06	2.16 ± 0.08	3.66 ± 0.19
TRPC3$^{(-/-)}$	vehicle	5	6.43 ± 0.25	2.73 ± 0.23[f]	2.47 ± 0.15
	ISO	6	5.83 ± 0.15	2.49 ± 0.07	2.79 ± 0.09[cg]
TRPC3/6$^{(-/-)}$	vehicle	6	6.77 ± 0.10	2.25 ± 0.06	2.87 ± 0.19
	ISO	7	6.36 ± 0.17	2.43 ± 0.12	2.93 ± 0.15

Genotype	Treatment	n	Organ weight per BW (mg/g)		
			Gas	Sol	Quad
WT	vehicle	10(9)*	3.84 ± 0.06	0.167 ± 0.007	6.04 ± 0.10
	ISO	11	4.23 ± 0.07[b]	0.211 ± 0.005[b]	6.52 ± 0.10
TRPC6$^{(-/-)}$	vehicle	6	4.11 ± 0.06	0.212 ± 0.007[bh]	6.12 ± 0.11
	ISO	7	4.62 ± 0.05[cf]	0.275 ± 0.009[dfko]	6.68 ± 0.04
TRPC3$^{(-/-)}$	vehicle	5	4.11 ± 0.10	0.174 ± 0.010	6.37 ± 0.10
	ISO	6	4.50 ± 0.09	0.206 ± 0.009	6.69 ± 0.23
TRPC3/6$^{(-/-)}$	vehicle	6	4.07 ± 0.05	0.184 ± 0.005	6.32 ± 0.09
	ISO	7	4.38 ± 0.13	0.221 ± 0.006[l]	6.60 ± 0.19

Genotype	Treatment	n	Organ weight per BW (mg/g)	
			TA	EDL
WT	vehicle	10	1.289 ± 0.023	0.276 ± 0.011
	ISO	11	1.443 ± 0.031[b]	0.290 ± 0.006
TRPC6$^{(-/-)}$	vehicle	6	1.460 ± 0.025[b]	0.310 ± 0.010
	ISO	7	1.633 ± 0.030[de]	0.316 ± 0.006[n]
TRPC3$^{(-/-)}$	vehicle	5	1.380 ± 0.022	0.282 ± 0.006
	ISO	6	1.591 ± 0.029[i]	0.286 ± 0.007
TRPC3/6$^{(-/-)}$	vehicle	6	1.350 ± 0.023	0.292 ± 0.004
	ISO	7	1.514 ± 0.053[l]	0.273 ± 0.006

*Gas, Quad n=10, Sol n=9

Table 6. Body weight and organ weight per body weight of mice treated with ISO for 4 weeks.

BW, Body weight; Gas, Gastrocnemius muscle; Sol, Soleus muscle; Quad, Quadriceps muscle; TA, Tibialis anterior muscle; EDL, Extensor digitorum longus muscle. Data are shown as mean ± SEM. Significance was determined by one-way ANOVA followed by Tukey's comparison test. The results of heart weight were same as shown in Fig.13E. [a] $P<0.05$ compared with WT vehicle group, [b] $P<0.01$ compared with WT vehicle group, [c] $P<0.05$ compared with WT ISO group, [d] $P<0.01$ compared with WT ISO group, [e] $P<0.05$ compared with $TRPC6^{(-/-)}$ vehicle group, [f] $P<0.01$ compared with $TRPC6^{(-/-)}$ vehicle group, [g] $P<0.05$ compared with $TRPC6^{(-/-)}$ ISO group, [h] $P<0.05$ compared with $TRPC3^{(-/-)}$ vehicle group, [i] $P<0.01$ compared with $TRPC3^{(-/-)}$ vehicle group, [j] $P<0.05$ compared with $TRPC3^{(-/-)}$ ISO group, [k] $P<0.01$ compared with $TRPC3^{(-/-)}$ ISO group, [l] $P<0.05$ compared with $TRPC3/6^{(-/-)}$ vehicle group, [m] $P<0.01$ compared with $TRPC3/6^{(-/-)}$ vehicle group, [n] $P<0.05$ compared with $TRPC3/6^{(-/-)}$ ISO group, [o] $P<0.01$ compared with $TRPC3/6^{(-/-)}$ ISO group.

Acknowledgements

I would like to express my deep gratitude to Professor M. Nishida (Kyushu University, National Institute for Physiological Sciences [NIPS] and SOKENDAI) for passionate mentoring. He always encouraged me and gave me a lot of opportunities to improve myself.

I also would like to show my great appreciation to Professor S. Adachi-Akahane (Toho University), Professor Y. Minokoshi (NIPS/SOKENDAI) and Dr. Y. Fukata (NIPS/SOKENDAI) for constructive discussion and warm encouragement.

I am deeply grateful to Dr. Y. Yamaguchi and Professor G. Iribe (Asahikawa Medical University) for providing data of change in cariomyocyte sarcomere length and giving insightful comments.

I would like to thank Dr. Y. Sato and Dr. T. Kuroda (National Institute of Health Sciences) for performing microarray assay.

I am grateful to Professor K. Jalink (The Netherlands Cancer Institute) for gifting Epac-based FRET biosensor.

I would like to thank Spectrography and Bioimaging Facility (NIBB Core Research Facilities) for technical support of confocal imaging.

I also thank Section of Instrument Design Room (NIPS) for making the setting of cardiomyocyte Ca^{2+} imaging.

This research was partly supported by JSPS KAKENHI Grant Number JP19J14538.

I would like to offer my special thanks to all lab members in Division of Cardiocirculatory Signaling (NIPS) and Department of Physiology (Kyushu University). Without their guidance and tremendous support, this project would not have been possible.

Finally, my heartfelt appreciation goes to my family for continuing support and constant encouragement.